



Eidgenössische Technische Hochschule Zürich  
Swiss Federal Institute of Technology Zurich



Institut für Werkzeugmaschinen und Fertigung  
Institute of Machine Tools and Manufacturing

# **Development of a Low-Cost Modal Analysis System**

Roman Rüttimann

Master Thesis

Nino Ceresa  
Prof. Konrad Wegener

Institute of Machine Tools and Manufacturing



# **Abstract**

Experimental modal analysis in tandem with the modal model of a machine tool is a powerful tool for the evaluation of the machine tools' dynamic behavior. But because experimental modal analysis is an expensive procedure, both due to high instrument costs and the need for experienced operators, the modal model is often not verified.

With the aim to decrease instrument costs and increase the use of experimental modal analysis, the system presented in this thesis consists of a micro controller based data acquisition system, a modal impact hammer and a low-cost accelerometer. The latter is a capacitive micro-electro-mechanical-sensor and the impact hammer is using a strain gauge load cell as impact sensor.

For the implementation of a low-cost modal analysis system based on the aforementioned components a micro controller based bus system and a specialized communication protocol is suggested.



# **Zusammenfassung**

Die experimentelle Modalanalyse, in Kombination mit dem modalen Modell einer Werkzeugmaschine, ist ein mächtiges Werkzeug, um das dynamische Verhalten der Werkzeugmaschine zu evaluieren. Teure Messinstrumente und der Bedarf an erfahrenen Bedienern machen die experimentelle Modalanalyse allerdings zu einem kostspieligen Unterfangen. Oft wird daher das modale Modell gar nicht validiert.

Mit dem Ziel die Kosten für Messinstrumente zu senken und den Gebrauch von experimenteller Modalanalyse zu steigern, wird in dieser Arbeit ein System vorgestellt, welches aus einem Mikrokontroller-basierten Datenakquisitionssystem, einem Impulshammer und einem kostengünstigen Beschleunigungssensor besteht. Letzterer ist ein kapazitiver mikro-elektronisch-mechanischer Sensor und der Impulshammer ist mit einer Dehnmessstreifen basierten Ladungszelle ausgestattet.

Für die Umsetzung eines kostengünstigen Modalanalysesystems auf der Grundlage der zuvor genannten Komponenten, wird ein Mikrokontroller-basiertes Bus-System mit einem spezialisierten Kommunikationsprotokoll vorgeschlagen.



# Entwicklung eines Low-cost-Modalanalyse-Systems

Bachelor- / Masterarbeit

---

## **Problemstellung**

Mit zunehmender Verbreitung von simulationsgestützter Entwicklung wird auch der Bedarf nach Methoden zur Modellverifikation in der Industrie grösser. Die experimentelle Modalanalyse (EMA) ist ein mächtiges Werkzeug zur Validierung von Simulationsmodellen von Werkzeugmaschinen. Dabei wird die Struktur mittels Impulshammer angeregt und die Antwort mit Beschleunigungssensoren gemessen. Kommerziell erhältliche EMA-Systeme kosten jedoch schnell über 50'000 CHF und sind daher für die breite Anwendung nicht geeignet. Für die Modellvalidierung sind jedoch die Auflösung und die Abtastrate des Messsystems häufig weniger kritisch, was den Einsatz von günstigeren Komponenten zulassen würde.

Mit den heute erhältlichen MEMS-Beschleunigungssensoren (wie sie in jedem Smartphone verbaut werden) und Mikrocontroller-Plattformen (wie Arduino) ergibt sich die Möglichkeit, ein einfaches EMA-System aus sehr günstigen Komponenten zu entwickeln.

## **Aufgabenstellung**

Auf Basis von günstigen Sensoren und Mikrokontrollern, sowie freier open-source Software, soll ein preiswertes Messsystem zur Validierung von Simulationsmodellen entwickelt werden.

### **Arbeitspakete:**

- ▶ Festlegen der Anforderungen an das Messsystem
- ▶ Auswahl der Komponenten
- ▶ Entwicklung der Software zum Auslesen der Sensoren (Arduino)
- ▶ Evaluation der Auswertesoftware (open-source)
- ▶ Vergleich mit einem kommerziellen EMA-System
- ▶ Präsentation der Ergebnisse und Diskussion

**Aufteilung der Arbeit:** 70% Entwicklung/Programmierung, 20% Messen, 10% Bericht

**Anforderungen:** Erfahrung mit Programmierung; optimalerweise im Bereich Mikrocontroller (Arduino).

### **Kontakt:**

Nino Ceresa

PFA E 82

044 633 37 19

[ceresa@inspire.ethz.ch](mailto:ceresa@inspire.ethz.ch)



# Contents

<b>1</b>	<b>Introduction</b>	<b>1</b>
1.1	Motivation . . . . .	1
1.2	Related Work . . . . .	1
1.3	Overview . . . . .	2
<b>2</b>	<b>State of the Art</b>	<b>3</b>
2.1	Measurement . . . . .	3
2.1.1	Measurement and Instrumentation . . . . .	3
2.2	Sensors and Transducers . . . . .	4
2.2.1	Load Cells . . . . .	4
2.2.2	Accelerometers . . . . .	5
2.2.3	Piezoelectric Sensors . . . . .	7
2.2.4	Capacitive Accelerometers . . . . .	7
2.3	Signal Conditioning and Processing . . . . .	9
2.4	Experimental Modal Analysis . . . . .	10
2.4.1	Frequency Response Measurement . . . . .	10
2.5	Electronic Components . . . . .	11
2.5.1	Passive Components . . . . .	12
2.5.2	Active Components . . . . .	13
2.5.3	Applications . . . . .	13
2.5.4	Analog to Digital Converters . . . . .	13
2.5.5	Transmission Protocols . . . . .	13
<b>3</b>	<b>Signal Chain</b>	<b>15</b>
3.1	Excitation . . . . .	15
3.2	Amplification . . . . .	15
3.2.1	Operational Amplifier . . . . .	15
3.2.2	Mean Noise Figure and the Signal-to-Noise Ratio . . . . .	17
3.3	Filtering . . . . .	19
3.3.1	Passive Lowpass Filters . . . . .	20

3.3.2	Optimal Lowpass Filters . . . . .	22
3.3.3	Anti Aliasing Filter . . . . .	29
3.4	Analog to Digital Conversion . . . . .	30
<b>4</b>	<b>Data Acquisition and Software</b>	<b>33</b>
4.1	Data acquistion . . . . .	33
4.1.1	Building Blocks . . . . .	33
4.1.2	Interfaces . . . . .	34
4.1.3	Dataflow . . . . .	35
4.2	Software . . . . .	36
<b>5</b>	<b>Test Setups</b>	<b>39</b>
5.1	Hammer-Hammer Test . . . . .	39
5.2	Andromeda Measurement . . . . .	40
5.3	Other Test Setups . . . . .	40
<b>6</b>	<b>Results and Discussion</b>	<b>43</b>
6.1	Hammer-Hammer Test . . . . .	43
6.2	Andromeda Measurement . . . . .	43
6.3	Other Test Setups . . . . .	44
<b>7</b>	<b>Conclusion and Future Work</b>	<b>47</b>
7.1	Conclusion . . . . .	47
7.1.1	Deficiencies . . . . .	47
7.2	Future Work . . . . .	48
<b>A</b>	<b>Appendix</b>	<b>49</b>
<b>List of figures</b>		<b>57</b>
<b>List of tables</b>		<b>59</b>
<b>Bibliography</b>		<b>61</b>

# List of Abbreviations

<b>AAF</b>	Anti Aliasing Filter
<b>AMP</b>	Amplifier
<b>ADC</b>	Analog to Digital Converter
<b>ASCII</b>	American Standard Code For Information Interchange
<b>CPU</b>	Central Processing Unit
<b>DAC</b>	Data Acquisition
<b>EMA</b>	Experimental Modal Analysis
<b>FIFO</b>	First In, First Out
<b>FPGA</b>	Field Programmable Gate Array
<b>FRF</b>	Frequency Response Function
<b>MCU</b>	Microcontroller Unit
<b>MEMS</b>	Micro-Electro-Mechanical-Systems
<b>MT</b>	Machine Tools
<b>LC</b>	Load Cell
<b>LPF</b>	Lowpass Filter
<b>LSB</b>	Least Significant Bit
<b>OPA</b>	Operational Amplifier
<b>IN-AMP</b>	Instrumentation Amplifier
<b>I<sup>2</sup>C</b>	Inter-Integrated Circuit
<b>IC</b>	Integrated Circuit
<b>RS</b>	Recommended Standard
<b>SNR</b>	Signal-To-Noise-Ratio
<b>SPI</b>	Serial Peripheral Interface
<b>TF</b>	Transfer Function
<b>USB</b>	Universal Serial Bus



# 1

## Introduction

### 1.1 Motivation

The Experimental Modal Analysis (EMA) is a powerful tool for evaluating dynamic models of structures. Despite its extensive usage in the aerospace industry, in many other engineering fields the benefits of EMA are overshadowed by the initial investment and the operator costs of an EMA system. To enable Machine Tools (MT) manufacturers to test their products and validate their modal predictions. Progress in Micro-Electro-Mechanical-Systems (MEMS) technology enables the use of new generation of low-cost sensors in EMA.

### 1.2 Related Work

Considering the use of low-cost accelerometers in EMA specifically, a two-point vibration measurement system with a bandwidth of 500 Hz has been developed [3]. The authors Chan and Huang used this system to conduct a multiple-point vibration tests on a MT. Operating at lower frequencies, Beskyroun and Ma used MEMS based accelerometers to conduct an EMA on building structures. Because we aim for higher bandwidths in this thesis, the transmission protocols used in the previously mentioned works do not satisfy the required data transmission rates. Piana et al. developed a modal test system, which uses piezoelectric transducers that are typically used to tune musical instruments as response sensors [8]. Although giving an alternative option in the development of a low-cost system, this approach comes with two main drawbacks. Firstly, the sensors measure in one dimension only, compared to the now common three in accelerometer integrated circuits (ICs). Because of this, the system is unsuited for some use cases. Secondly, when using piezoelectric transducers, one needs to conduct dedicated signal conditioning for each sensor. In comparison, this is already integrated in accelerometer Integrated Circuit (IC)s that offer direct digital signal output. Hence more components must be used when going with the alternative option, increasing cost and form factor and decreasing reliability. Finally, a construction kit for a low-cost

### 1.3 Overview

vibration analysis system was proposed by Vollmer et al. back in 2009 [12]. According to this paper, a broad product line of capacitive accelerometer ICs, optimized for different bandwidths are available. But starting at a bandwidth of 2500 kHz and higher only accelerometer ICs with high acceleration ranges of  $\pm 70\text{ g}$  are available. For noise reduction, analog filters are sometimes partly or fully integrated. The noise in capacitive sensors can be expected to be in the range of 0.1...1 % of the measurement range, i.e. a factor of 100...1000 worse than in piezoelectric sensors.

In the field of civil engineering, bridges and skyscrapers require continuous vibration signal logging for structural health monitoring. This leads to an increased interest in driving down the cost of accelerometer based vibration monitoring systems. Girolami et al. has developed a low-cost MEMS systems for structural health monitoring of civil structures [5]. Typically, lower sensor bandwidths are required when analyzing building structures compared to MTs. The data rate of the proposed monitoring system does not suffice for this thesis.

Structural health monitoring is also required in rotary systems such as gas and wind turbines. Esu et al. integrated low-cost accelerometers in wind turbines and logged data via radio frequency to a central device [4]. An integration of digital accelerometer ICs with sampling rates of up to 1600 Hz has been tested under laboratory conditions.

Addressing low-cost impact hammer constructions, Waltham and Kotlicki implemented a piezoelectric transducer in a hammer, that is designed to trigger barbecue lighters [13]. The hammer was tested by impact against wooden planks. It yielded robust signal in a wide range of forces. In contrast to this work, the load cell used in this thesis is strain gauge base in order to be more cost-effective compared to the typical piezoelectric sensors used in impact hammers. For inexpensive calibration of a load cell used for modal testing, Wang et al. introduced practical techniques [14].

## 1.3 Overview

First fundamentals in measurement instrumentation, sensors and EMA is introduced in the state of the art. Then the Data Acquisition (DAC) developed for this project is presented in chapter 4. Testing environment are described in the chapter 5 and measurement results are discussed in results. Finally the conclusion gives reflects on the project.

# 2

## State of the Art

### 2.1 Measurement

The process of measurement is the comparison of data from the physical world in the frame of an agreed standard. It is carried out by using an instrument.

This section points to some key aspects of measurement instruments and components, used in the frame of this thesis. As a result some sections of [15] are summarized.

#### 2.1.1 Measurement and Instrumentation

Measurement instruments translate signals from the physical world into an agreed upon standard. These standardized signals can be compared, altered and stored. The original data acquired from the physical signal is usually in analog form. This is then converted to digital before it is passed on. The signal chain of a typical digital measurement instrument is shown in Figure 2.1.

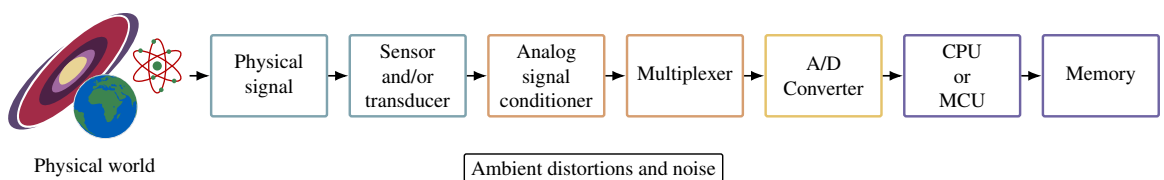


**Figure 2.1:** Digital measurement instrument

## 2.2 Sensors and Transducers

A device that responds to a changing phenomenon is called sensor. If we need to transfer from one energy from to another, we use a device called transducer. If one compares sensors and transducers based on the energy input and output, one identifies three types:

- In *modifiers* a specific energy form is not converted but modified. Hence they use the same form of energy as input and output.
- *Self-generators* give out electric signals from non-electric inputs without the need of additional energy.
- *Modulators* in contrast give out electric signals from non-electric inputs, but require an additional energy input.

As part of this we focus on self-generating piezoelectric sensors, capacitive modulators that convert mechanical deformation in a static electric field into an electric current, as well as strain gauge based modulators.

### 2.2.1 Load Cells

A force measurement sensor that converts a force into an electrical signal is called Load Cell (LC). The basis of force measurement results from the physical behavior of a body under external forces. Depending on the bandwidth and magnitude of the signal, as well as the duration of the signal capture, different methods of force measurement are applied in various designs. The methods in brief are:

- Balancing the unknown force against a standard mass through a system of levers
- Measuring the acceleration of a known mass
- Equalizing it to a magnetic force generated by the interaction of a current-carrying coil and a magnet
- Distributing the force on a specific area and then measuring the pressure
- Converting the applied force into the deformation of an elastic element

Furthermore, these methods yield numerous of designs of measuring equipment. Each of which addressing two main problems. First, the physical and geometrical constrains by the application of the device and second, the means by which the force can be converted into an electrical signal.

LCs in EMA equipment designs typically use piezoelectric sensors because of their high bandwidth in compact designs and their capability to detect small deflections.

### Strain Gauges

In strain gauge LCs the elastic properties of a material probe is exploited.

The probe is loaded in a controlled manner in its elastic region. Deformations are captured by a strain gauge at a suitable location. The probe deformation is directly determined by the force acting on the probe because of Hooke's law.

The strain gauges themselves each use a specific length gauge wire in order to reach a resistance of typically  $120\ \Omega$ . The wire is bonded between two thin sheets in coiled up form as can be seen in Figure 2.2a. The

sheets act as insulating carrier and can be easily deformed with the intent of passing the load to the wire grid. The gauge is attached to the probe structure by a wax or a resin. The intent is that deformations in transversal direction of the strain gauge act on all coils simultaneously, changing their resistance. By using small sized strain gauges with respect to the probe, the mechanical and thermal properties of the strain gauge become negligible small. As an example, we assume the probe expands. Then a strain gauge on its surface experiences tension. The coils in the grid are therefore stretched and as a result of the generalized Hook's law the coil cross sections decrease. Both the strain in axial direction of the coil and the decreased coil cross sections increase the wire's resistance.

In order to measure deformations one needs to take environmental influences into consideration. It is well known that resistance is susceptible to variations in temperature. Placing the strain gauge in a wheatstone bridge, with resistors, that change their resistance in the same manner as the strain gauge will reduce the influence of temperature significantly — see Figure 2.2b.

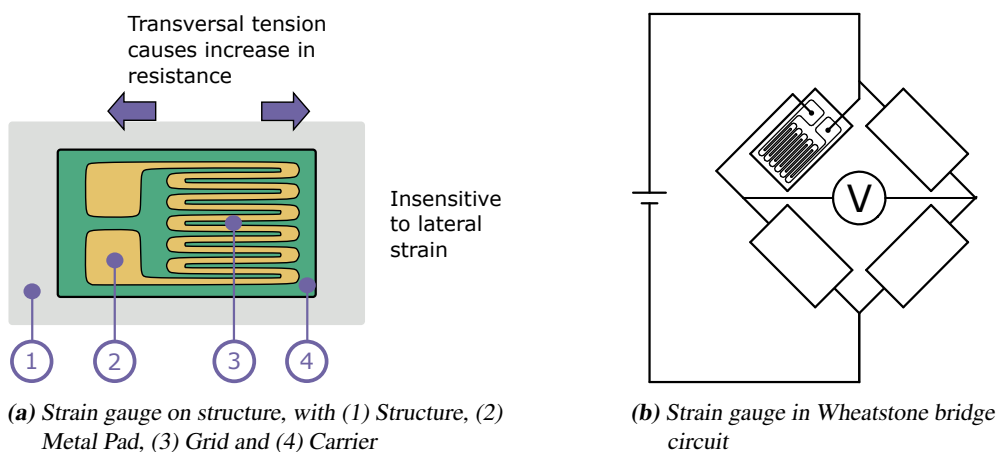


Figure 2.2: Strain gauge

## 2.2.2 Accelerometers

Accelerometers are sensors that convert acceleration into an electrical signal. In order to measure a physical phenomenon we use seismic masses that act on the sensor structure based on their inertia properties. In strain gauge based accelerometers the structure translates the inertia force into a deformation, where capacitive sensor structures may use deformations or relative motions of separate components in an electric field. In piezoelectric accelerometers the seismic mass deforms a piezoelectric material, see Figure 2.3.

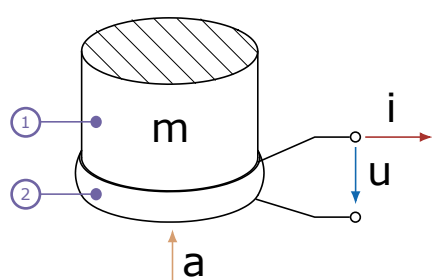


Figure 2.3: Function principle of a piezoelectric accelerometer

---

a	: Acceleration
m	: Mass
i	: Induced Current
v	: Induced voltage
(1)	: Seismic mass
(2)	: Piezoelectric material

---

Table 2.1: Legend to Figure 2.3

## 2.2 Sensors and Transducers

In seismic accelerometers the base of the arrangement is motion. When describing the one dimensional case, one can express non-stationary random vibrations acting on the accelerometer as

$$m \frac{d^2z}{dt^2} = c \frac{dz}{dt} + kz = mg \cos(\theta) - m \frac{d^2x_1}{dt^2} \quad (2.1)$$

where

$m$  is the seismic mass

$z = x_2 - x_1$  is the relative motion between the mass and the base

$x_1$  is the displacement of the base

$x_2$  is the displacement of the mass

$\theta$  is the angle between sense axis and gravity

The second-order system expressed in Laplace transform thus takes the form

$$G(s) = \frac{X(s)}{F(s)} = \frac{K}{s^2/\omega_n^2 + 2\zeta s/\omega_n + 1} \quad (2.2)$$

where

$s$  is the Laplace operator

$K = 1/k$  is the static sensitivity

$\omega_n = \sqrt{k/m}$  is the undamped frequency in rad/s

$\zeta = c/2\sqrt{km}$  is the damping ratio

It is obvious that the performance of accelerometers depends on their static sensitivity, the natural frequency and the damping ratio. We want the accelerometer to have a linear transfer function in the range of operation. But namely the damping ratio can distort a measurement when operating an accelerometer near its eigenfrequency, see Figure 2.4.

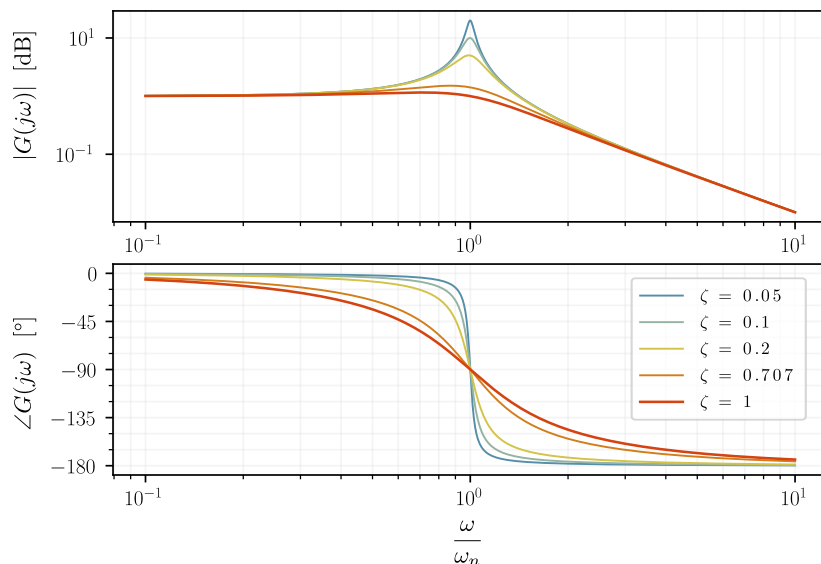


**Figure 2.4:** Bode plots of second order system describing the dynamic behavior of seismic accelerometers

### 2.2.3 Piezoelectric Sensors

Some materials develop electric charge proportional to directly applied mechanical stress. The same materials show the converse effect. A proportional strain of the material will occur to an applied electric field.

The first phenomenon has found its application in a variety of self-generating sensors that output electrical signals — namely in LCs and accelerometers, where the piezoelectric charge is converted into a current or voltage signal.

Piezoelectric sensors are designed to exploit the piezoelectric effect of the material in one axis. Additionally, we use amplifier circuits so that the weak electrical signal, induced due to the piezoelectric charge, is elevated to amplitudes that are in the range of operation of standard electronic components. These circuits require additional energy. Commercially available LCs therefore require supplied energy — see Figure 2.5.

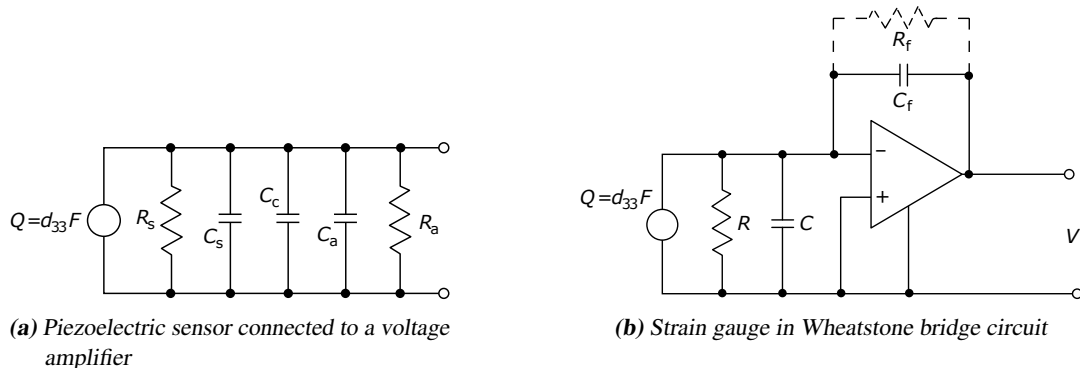


**Figure 2.5:** Piezoelectric sensors connected to amplifier circuits [15]

Depending on the design of the sensor, piezoelectric materials are used in different shapes. Figure A.1 shows some possible variations.

### 2.2.4 Capacitive Accelerometers

To understand the working principle of capacitive accelerometers, we first consider the displacement sensors.

#### Capacitive Displacement Sensors

The basic sensing element of a displacement sensor typically consists of two parallel electrodes with capacitance  $C$ .

$$C = f(d, A, \varepsilon) \quad (2.3)$$

With variable distance, dielectric material or area and with the measurement of the capacitance, we can then deduce the plate displacement in normal and parallel direction to the plates depending on the method used. See Figure 2.6

## 2.2 Sensors and Transducers

In variable displacement sensors, the distance between two capacitive plates is inversely proportional to the capacitance.

$$C(x) = \frac{\varepsilon A}{x} = \frac{\varepsilon_r \varepsilon_0 A}{x} \quad (2.4)$$

where

$\varepsilon$  is dielectric constant or permittivity

$\varepsilon_r$  is the relative dielectric constant (in air and vacuum  $\varepsilon_r \approx 1$ )

$\varepsilon_0$  is 8.854 188 F/m, the dielectric constant of vacuum

$x$  is the distance of the plates in m

$A$  is the effective area of the plates in  $\text{m}^2$

In variable area displacement sensors, the capacitance is proportional to the reduction of area due to the movement of the plate.

$$C(x) = \frac{\varepsilon_r \varepsilon_0 (A - wx)}{d} \quad (2.5)$$

where

$\varepsilon_2$  is the permittivity of the displacing material (e.g. liquid)

$w$  is the width

$wx$  is the reduction in the area due to movement of the plate

$d$  is the distance of the plates in m

In variable dielectric sensors, the capacitance depends on the ratio of each permittivity in the electric field.

$$C(x) = \varepsilon_0 w [\varepsilon_2 l - (\varepsilon_2 - \varepsilon_1)x] \quad (2.6)$$

$$(2.7)$$

where

$x$  is the displacement normal to the plate's direction

$\varepsilon_1$  is the relative permittivity of the dielectric material

$\varepsilon_2$  is the permittivity of the displacing material (e.g. liquid)

Differential capacitive displacement sensors are setup in capacitive arrangements that aim to eliminate nonlinearities. Different variations of these types of sensors exist. For example we can allow the outer plates to move and fix the middle one or we can reverse this setup. But the range is equal to twice the separation in both cases.

$$2\delta C = C_1 - C_2 = \frac{\varepsilon_r \varepsilon_0 lw}{d - \delta d} - \frac{\varepsilon_r \varepsilon_0 lw}{d + \delta d} = \frac{2\varepsilon_r \varepsilon_0 lwd}{d^2 + \delta d^2} \quad (2.8)$$

$$C_1 + C_2 = \frac{\varepsilon_r \varepsilon_0 lw}{d - \delta d} + \frac{\varepsilon_r \varepsilon_0 lw}{d + \delta d} = \frac{2\varepsilon_r \varepsilon_0 lwd}{d^2 + \delta d^2} \quad (2.9)$$

$$(2.10)$$

Giving approximately

$$\frac{\delta C}{C} = \frac{\delta d}{d} \quad (2.11)$$

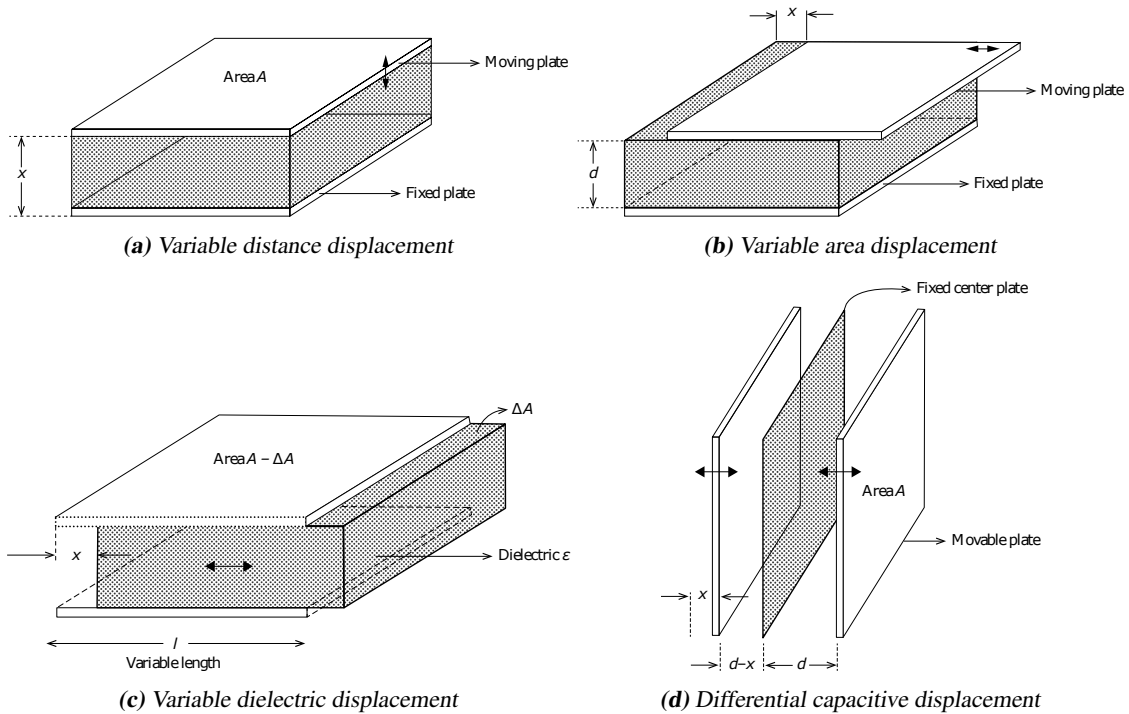


**Figure 2.6:** Capacitive displacement sensors [15]

### From Displacement to Acceleration

If one combines a capacitive displacement sensor with a seismic mass, one can use the inertia force to correlate the acceleration to the displacement and hence to the change in the electric field of the sensor. With the use of differential capacitive designs and high machining accuracy these designs can be realized in a tiny form factor as Micro-Electro-Mechanical-Systems (MEMS). A scheme of such a sensor is shown in Figure 2.7.

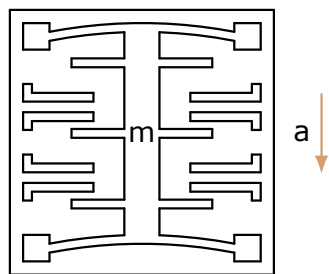


**Figure 2.7:** Capacitive MEMS accelerometer, with acceleration  $a$  and the seismic mass  $m$ . The bridges attached to the seismic mass act as dielectricum.

## 2.3 Signal Conditioning and Processing

In an ideal world, the signal output of a sensor would correlate to the measurand exactly. In real systems this is not the case because of a variety of reasons. In low-frequency applications, the most important ones are:

## 2.4 Experimental Modal Analysis

- The voltage or current rating at a sensor's output is not perfectly linear with respect to the measurand. Often the output is pseudo-linear in a limited range of values and deviates from the trajectory for values outside of this range.
- Noise and shifts introduced through the inherent impedances of analog components lead to deviations from the voltage or current rating of the sensor as well as deviations of these ratings with respect to the measurand itself.
- The quantization process causes the captured value space to have a finite resolution.
- Analog signals can only be digitized with a finite sampling rate. A discrete set of data points is captured instead of a continuous signal.

The field of signal processing includes analyzing, modifying and synthesizing signals. Most prominently, in data acquisition systems we convert analog signals to digital ones that can be further processed without the parasitic effects of the analog realm. On the opposite side when addressing these parasitic effects one needs to apply signal conditioning. In other words, before every processing step of an analog signal we need to consider signal conditioning. When dealing with digital signals, no signal conditioning is required.

## 2.4 Experimental Modal Analysis

EMA is a powerful tool to detect vibration related problems of mechanical structures. We use modes to characterize resonant vibrations of the system. This section is only a short excerpt of an introduction to EMA. An overview has been presented by Schwarz and Richardson in [9].

### Vibration

In every vibration one can observe a combination of two different types of vibrations. The forced and the resonant ones. Forced vibrations in a structure are caused by

- Internally generated forces
- Unbalances
- External loads
- Ambient excitations

Common examples of vibration sources in MT are displayed in Figure 2.8.

Resonant vibration arises when one or more of the natural modes of vibration, inherent properties of the structure under investigation, is excited. Resonant vibration typically amplifies the vibration response to a level that exceeds deflection, stress and strain caused by static loading.

### 2.4.1 Frequency Response Measurement

In an EMA one needs to determine the Frequency Response Function (FRF) from input to output. To achieve this we measure the so called response or output function of the structure under investigation. The measurement instrument for this task uses a signal chain in form of 2.9.

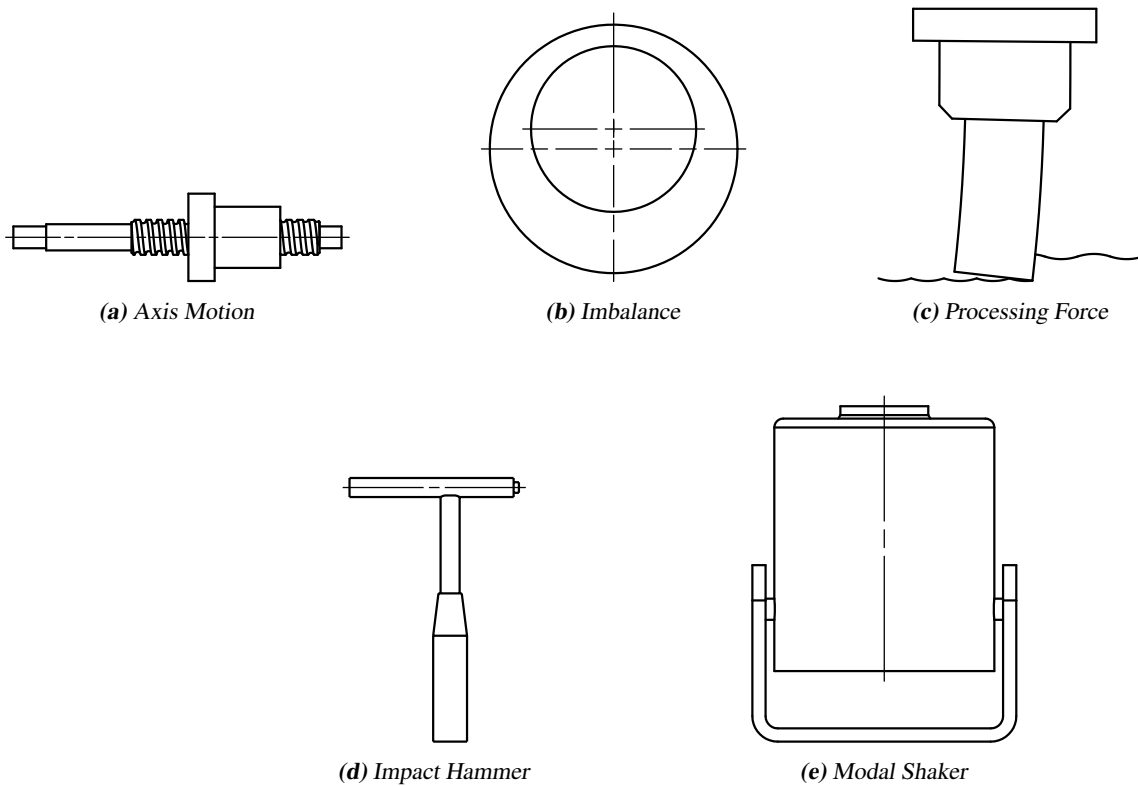


**Figure 2.8:** Sources of forced vibration. Note that (a), (b) and (c) occur during MT operation, while (d) and (e) are devices that are explicitly used for EMA to introduce vibrations into the structure of investigation.

- The sensor on the structure translates the physical value (acceleration, velocity or position) into an electrical voltage or current, the analog signal variable.
- The amplifier amplifies the typically low power signal to fit it to the input range of the Analog to Digital Converter (ADC).
- The ADC samples and quantizes the analog signal. It is then converted into a digital signal, in which the quantity is expressed in form of a binary code.
- The discrete time signal is then stored on the computer memory.

## 2.5 Electronic Components

This section serves as an introduction to the function of selected electronic components and circuits. It does not give a complete overview of the state of the art. For more background on electronics [10] and [11] may be consulted.

Electronic components are divided into two main types; passive and active ones. Where active components are allowed to generate, amplify or oscillate an electrical signal, passive components can only absorb, dissipate or store electric energy.

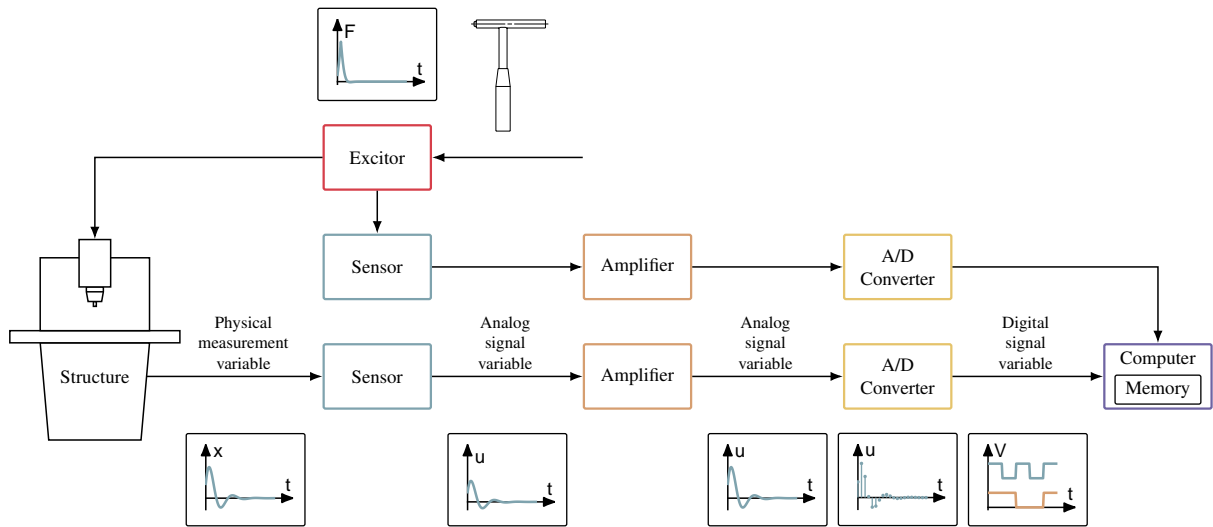


Figure 2.9: FRF measurement setup

### 2.5.1 Passive Components

Because of the increase in digital processing, the number of passive components has decreased drastically in modern electronic circuits. This, in addition to the trend of using more complex devices in favour to multiple simple passive components, has led to a great variety of passive components which are designed with emphasis on reliability.

Typical examples of passive components are:

**Wires** Depending on the mechanical requirements for the wire, it can either be designed with a solid core or a stranded wire core. A wire consisting of multiple smaller diameter conductors shows better flexibility but reduced current-carrying capacity at the same wire diameter. This is because of the smaller overall conductor cross-section of a stranded wire and, when transmitting high frequency signals, a greater power dissipation due to the more prevalent skin effect. Furthermore the simplicity of solid core wires makes them more resistant to corrosion and more suitable to be used in harsh environments.

**Resistors** Depending on the application different types of resistors can be applied. Fixed value resistors, can be used for safety of other components by dissipating heat or reducing to set the current and voltage in combination relative to other devices. Variable resistors change their value due to different physical phenomena. Thermistors show resistances that are highly susceptible to temperature changes, potentiometers resistance is manually tunable and photoresistors show a light dependant resistance, to name a few.

**Capacitors** Capacitors store energy in form of an electric field. They have many applications, most prominently in filter circuits and as bypass capacitors to reduce smooth out non constant power draws.

**Inductive Devices** Are devices that store energy in form of an electric field. In modern devices coils are less common due to benefits, when realizing the circuit with capacitors instead. But in specialized applications, namely when converting between electrical and mechanical signals, i.e. in motors, generators, loudspeakers etc.

## 2.5.2 Active Components

Active components show some form of amplification of the input signal in most cases; in other ones they generate vibrations, but generally an additional energy supply is needed to operate active components.

As an essential example, we consider the Operational Amplifier (OPA). The OPA is a multi-stage, high gain and galvanically coupled differential amplifier. It is used to amplify an electrical signal, and its function is primarily determined by its surrounding circuit. Namely filters can be realized by using OPAs.

## 2.5.3 Applications

Electrical signal conditioning is based on arrangements of active and passive components in circuits. A good and in depth coverage of active filters and measurement circuits can be found in [11]. For many common applications a Integrated Circuit (IC) exists. These circuits internal to chips that come in various package sizes, see Figure A.2.

## 2.5.4 Analog to Digital Converters

## 2.5.5 Transmission Protocols

Digital transmission protocols offer established standards for the communication between ICs and devices that at least include a processing unit. There exists a plethora of protocols, that address the communication on a range of different levels of abstraction. Theoretically, these levels can be categorized according to the Operational Amplifier model (OPA model), but it is obvious that most protocols address issues on multiple levels. Nevertheless, the model is useful when establishing a new network, since all steps, necessary for a successful communication, are best traced in order of the model. The OPA model includes seven layers, as seen in Figure 2.10.

1. The *physical layer* defines the physical form of the data transmission, i.e. the medium, in which the data is transmitted and the physical connections.
2. The *data link layer* addresses the transmission conditions and standards, which allow the communication between two or more devices.
3. In the *network layer* we implement the definitions for the shortest connections, error detection and addressing techniques.
4. The *transport layer* ensures that all data is transparent and securely transmitted. Its segmented data is used to detect duplicates and missing data.
5. The *session layer* establishes channels between devices. It manages open connections and synchronization.
6. It is the *presentation layer*, where one defines the syntax and semantics of the code.
7. And the *application layer* that provides the protocols and services that are used in applications. This is the data directly available to the end-user.

When dealing with real hardware, the level of abstraction that can be reached will be limited depending on the device. Namely in the communication between Microcontroller Unit (MCU)s the Different low end communication protocols can be used to communicate between ICs. Many smart devices of today

## 2.5 Electronic Components

use the Inter-Integrated Circuit ( $I^2C$ ), the Serial Peripheral Interface (SPI) or both connections to access their registers. With these protocols two respectively, four wires connect two devices over short distances. When the distance increases or the environment gets to noisy, one needs to improve the cable's isolation, insert active signal repeaters, or switch to another transmission standard. The transmission standard RS-485, defines a widely adopted industry standard of differential digital signal transmission. These offer more stable signal transmissions in harsh environments and over long distances with the caveat of using two wires for each signal. In depth information about data communication protocols is available in the handbook [2] Rs intro [7]

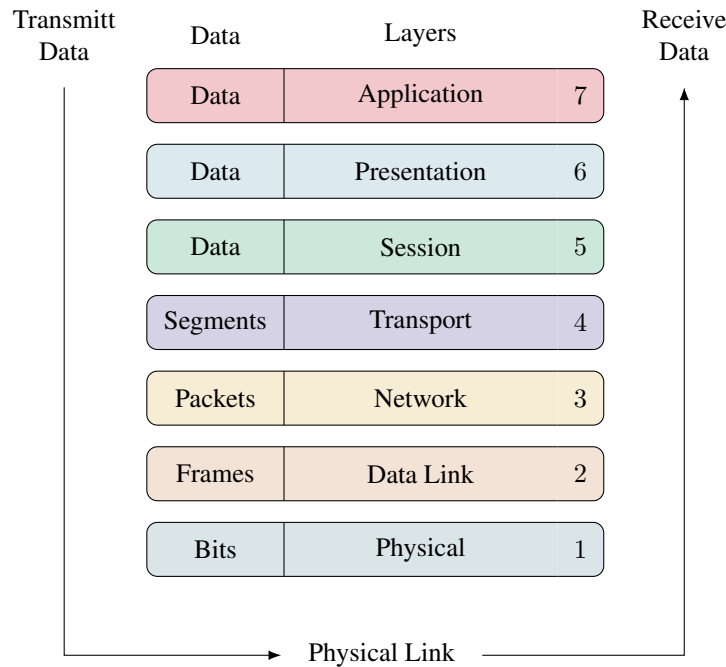


**Figure 2.10:** OSI Model

### RS-458

Recommended Standard (RS)-485

### Serial Peripheral Interface

SPI

### USB

Universal Serial Bus (USB)

# 3

## Signal Chain

Some sensors operate at small energies. The signals are too weak to be converted into digital ones by standard components. *Signal conditioning* enables us to amplify and denoise analog signals so that the signal can be further processed. In our application, both the load cell's and accelerometer's sensors signal must be amplified to match the input range of the respective ADC. In this section we put together all conditioning steps necessary from sensor to the digital signal under the term signal chain. Because the selected accelerometers come in an IC packages that include the complete signal chain, we focus on the signal chain of the load cell. For more background on signal conditioning and processing, read Section 2.3.

### 3.1 Excitation

### 3.2 Amplification

Electrical signals are amplified by active electrical components; i.e. typically by OPAs or circuits of OPAs.

#### 3.2.1 Operational Amplifier

Amplifiers apply signal gain on electrical inputs so that the output matches the input times a constant gain factor. The latter is determined by the impedance of the subsequent device in the signal chain and the magnitude at the input. But by setting the gain factor one predetermines the introduced absolute noise due to the amplifier's Signal-To-Noise-Ratio (SNR).

In simple amplifiers, the SNR purely depends on the quality of the components and the environmental conditions. This can be bypassed by building differential setups, where amplifiers, like transistors and field transistors, are fed with both the non-inverted and the inverted input signal individually. With multi-staging

### 3.2 Amplification

and additional filter circuits one can reduce the noise further and ultimately the SNR becomes strongly dependent on the circuit design and less dependent on the quality of each component. Specific to different applications, many variants of the described circuitry are available in so-called Operational Amplifiers (OPAs).

	Voltage output	Current output
Voltage input	<p>Standard OPA VV-OPA</p> $V_o = A_D V_D$	<p>Transconductance amplifier VC-OPA</p> $I_o = g_{m,D} V_D$
Current input	<p>Transimpedance amplifier CV-OPA</p> $V_o = I_N Z = A_D V_D$	<p>Current amplifier CC-OPA</p> $I_o = k_I I_N = g_{m,D} V_D$

**Figure 3.1:** Main operational amplifier types

OPAs are available in a variety of IC packages and differ little from discrete transistors in terms of size and price. In some packages even multiple individual OPAs are included. Initially OPAs offered high accuracy at low frequencies. Over time different circuit designs for different needs have broadened the field of application considerably. Today, it is hard to find a task that is better met by a transistor than by an OPA. We subdivide the latter into four main types, as shown in Figure 3.1. The differences are high-resistive or low-resistive inputs and outputs. The standard OPA and the transconductance amplifier, for example, have high-resistance inputs. Therefore, they are voltage controlled. The outputs on the other hand are of low and high internal resistance respectively, where low-resistance outputs act as voltage sources and high-resistance outputs act as current sources. In the naming convention the two leading letters represent input and output. “V” at first position stands for a voltage controlled OPA with a high-resistance input, where “C” means current controlled and low-resistive input. At the second position “V” and “C” define low- and high-resistance outputs that act as voltage and current source respectively. The differential gain of an ideal VV-OPA is given by the slope at the operating or bias point:

$$A_D = \left. \frac{dV_o}{dV_D} \right|_b \quad (3.1)$$

The transfer characteristics of an ideal OPAs can be seen in Figure 3.2. When dealing with current outputs the differential transconductance  $g_{m,D}$  indicates the degree of output current increase with rising input voltage.

$$g_{m,D} = \left. \frac{dI_o}{dV_D} \right|_b \quad (3.2)$$

Although the major part of electronics is based on voltage controlled circuits, the amplifiers with low-resistance inputs are better suited for high frequency applications. The main advantages of the latter are the lower oscillation tendency due to shortened internal signal paths and larger range of possible gains

compared to high-resistance input OPAs. When designing circuits with current amplifiers it is often easier to use the current transfer factor  $k_I$  than the differential transconductance.

$$k_I = \frac{dI_o}{dI_N} \Big|_b \quad (3.3)$$

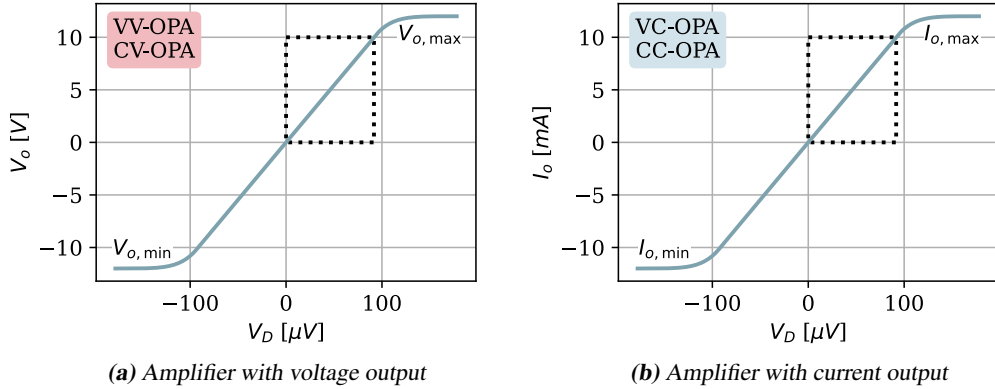


**Figure 3.2:** Transfer characteristics of OPAs, where the dotted square includes the line of positive operating or bias points.

Because of their differential circuit, OPAs normally are powered by symmetric operating voltages. Rail-to-rail OPAs have the capability to control the output between the positive and negative supply voltage, allowing maximal amplification, see Figure 3.3. When working with digital circuits, a single voltage supply is preferred. For this case one uses single supply voltage OPAs.

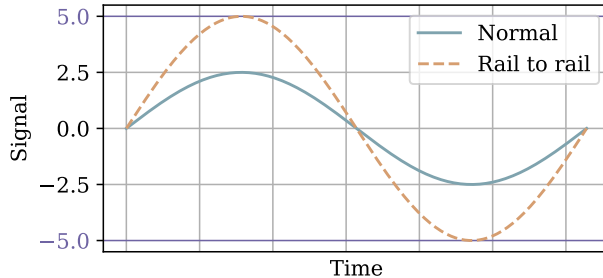


**Figure 3.3:** OPA controllability at  $\pm 5$  V operating voltage

### 3.2.2 Mean Noise Figure and the Signal-to-Noise Ratio

To determine the mean noise figure and the Signal-To-Noise-Ratio (SNR) one needs conduct tests on an amplifier with a known signal. In its simplest form one can determine the SNR and the mean noise figure by connecting a signal generator directly to the amplifier's input. Per definition, the SNR is the ratio of the information containing signal power over the noise power:

$$\text{SNR} = \frac{P_{us}}{P_n} \quad (3.4)$$

### 3.2 Amplification

where  $P_n$  is the power in the application specific frequency interval  $f_L < f < f_U$ . We know that the power is proportional to the square of its effective value. The effective value, on the other hand, is defined as the root-mean-square of the electrical signal. Hence the noise of the signal generator is:

$$\text{SNR}_g = \frac{\nu_{g,\text{eff}}^2}{\nu_{r,\text{eff}}} = \frac{\nu_{g,\text{eff}}^2}{\int_{f_L}^{f_U} |\boldsymbol{\nu}_{r,g}(f)|^2 df} \quad (3.5)$$

An amplifier increases the noise density by the *spectral noise figure*  $F(f)$ . The SNR at the amplifier input is thus:

$$\text{SNR}_i = \frac{\nu_{g,\text{eff}}^2}{\nu_r} = \frac{\nu_{g,\text{eff}}^2}{\int_{f_L}^{f_U} |\boldsymbol{\nu}_r(f)|^2 df} = \frac{\nu_{g,\text{eff}}^2}{\int_{f_L}^{f_U} F(f) |\boldsymbol{\nu}_{r,\text{eff}}(f)|^2 df} \quad (3.6)$$

which is lower than the SNR of the signal generator.

The *mean noise figure* corresponds to the relation of the SNR ratios:

$$F = \frac{\text{SNR}_g}{\text{SNR}_i} = \frac{\int_{f_L}^{f_U} F(f) |\boldsymbol{\nu}_{r,g}(f)|^2 df}{\int_{f_L}^{f_U} |\boldsymbol{\nu}_{r,g}(f)|^2 df} \quad (3.7)$$

And is usually quoted in decibels dB

$$F_{\text{dB}} = 10 \log F \quad F_{\text{dB}} = \text{SNR}_{g,\text{dB}} - \text{SNR}_{g,\text{dB}} \quad (3.8)$$

When using an ideal signal generator, that has uniform noise density over all frequencies, (3.7) simplifies to:

$$F = \frac{1}{f_U - f_L} \int_{f_L}^{f_U} F(f) df \quad (3.9)$$

Additionally, one can often assume the noise figure to be constant. Thus  $F = F(f)$ , which is generally referred to as the noise figure  $F$ .

In some applications the noise causes stronger interference in certain ranges of the given frequency interval than in other ranges. Then a weighted filter, whose absolute frequency response is proportional to the disturbing effect, is used to get more meaningful SNRs. For this the noise density of the generator in the denominators of Equations 3.5 and 3.6 are replaced by the *weighted noise density*:

$$|\boldsymbol{\nu}_{r(B),g}(f)|^2 = \left| \vec{H}_B(2j\pi f) \right|^2 |\boldsymbol{\nu}_{r,g}(f)|^2 \quad (3.10)$$

with the transfer function of the weighted filter  $\boldsymbol{H}_B(s)$ .

Note that the bandwidth of the amplifier needs to cover at least the interval of the useful signal  $f_L < f < f_U$  to provide equal amplification. Moreover, the bandwidth of the amplifier is usually wider than required, i.e. it amplifies the ranges  $f < f_L$  and  $f > f_U$  with operating gain  $\boldsymbol{A}_B(s)$ . It is in these ranges, where the signal only contains noise. Which means, that the amplifier, if not limited to the frequency range, provides the noise power at the output:

$$P_{n,o} = \int_0^\infty |\boldsymbol{A}_B(2j\pi f)|^2 F(f) |\boldsymbol{\nu}_{r,g}(f)|^2 df \quad (3.11)$$

Considering that the signal is amplified by the useful gain  $A_{B,us}$ , which is assumed to be constant over the useful range, the SNR at the amplifier output becomes:

$$\text{SNR}_o = \frac{|A_{B,us}|^2 \nu_{g,\text{eff}}^2}{P_{n,o}} = \frac{|A_{B,us}|^2 \nu_{g,\text{eff}}^2}{\int_0^\infty |A_B(2j\pi f)|^2 F(f) |\nu_{r,g}(f)|^2 df} \quad (3.12)$$

Which is lower than  $\text{SNR}_i$ , given by (??), since  $P_{n,o}$  includes the total noise, compared to the range  $f_L < f < f_U$  used to define in  $P_{n,i}$ . Note that the components following the amplifier are primarily driven by the amplified noise, if the power at the output  $P_{n,o}$  is considerably larger than the useful signal power. That said, the noise of the  $P_{n,o}$  as defined in (3.11) is only of importance if the noise outside the useful range is transmitted. To reduce this signal component we apply a filter that reduces the bandwidth of the signal. Optimally this is a bandpass filter with lower and upper cutoff frequencies at  $f_L$  and  $f_U$ .

If the noise densities of both the signal generator and the amplifier are almost constant in the transfer bandwidth, the noise power at the amplifier output can be approximated by:

$$P_{n,o} \approx F |\nu_{r,g}|^2 \int_0^\infty |A_B(2j\pi f)|^2 df = F |\nu_{r,g}|^2 |A_{B,us}|^2 B_r \quad (3.13)$$

Where we defined the *equivalent noise bandwidth* as:

$$B_r = \frac{\int_0^\infty |A_B(2j\pi f)|^2 df}{|A_{B,us}(2j\pi f)|^2} = \frac{|A_B|^2}{|A_{B,us}|^2} f_L f_U \quad f \text{ (linear)} \quad (3.14)$$

This means that the area under the plot of the squared magnitude is replaced by the area of rectangle shown in Figure 3.4, i.e. the squared constant gain  $|A_{B,us}|^2$  times the equivalent noise bandwidth  $B_r$ .

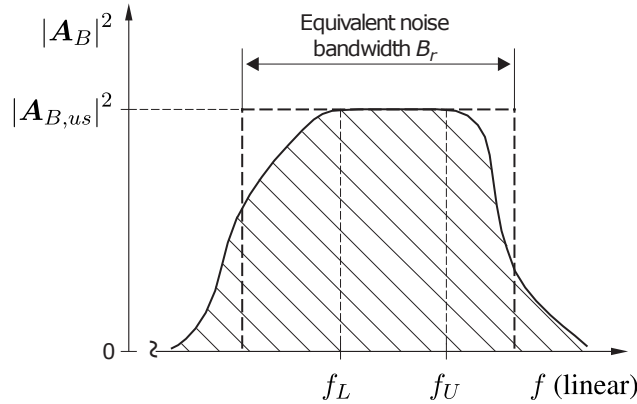


**Figure 3.4:** Equivalent noise bandwidth of an amplifier [11]

### 3.3 Filtering

Whenever we measure a signal in the real world, it will inherently contain some form of noise. Filtering enables us to cut off contributions to the signal amplitude, that are outside the useful signal frequency bandwidth.

The two main types of filters are analog and digital ones, where the digital filters are more versatile, cost-effective and precise compared to their counterpart. Nevertheless, analog filters are required when

### 3.3 Filtering

dealing with analog signals, i.e. whenever the signal must be bandwidth limited. As described previously, it is advantageous if a signal is bandwidth limited before it is amplified, because we do not want to amplify the noise components of the signal. Furthermore electric devices in the signal chain may be bandwidth limited as well; disturbances of the signal occur due to frequency dependent phase shifts or damping when operating outside these ranges. Namely when digitizing a signal, the additional effect of aliasing may disturb a signal significantly if it contains frequency components above the Nyquist frequency.

We operate at a low frequencies in the frame of this thesis. The useful bandwidth of the lower modes in EMA of MTs range typically between a few ten and a few hundred hertz. Therefore, we focus on a lowpass-filter design, so that there is no miss on the lowest eigenfrequencies. For simplicity, from this point on onward the term bandwidth addresses the upper bandwidth limit, while the lower limit remains near zero. Additionally, the cutoff frequency refers to the lowpass cutoff frequency. For more details on other filter designs we recommend the textbooks for analog electronics and filter design [11], [10], [16]. The content in this Section is reliant on the theories, found in these books.

#### 3.3.1 Passive Lowpass Filters

The frequency response of the simplest Lowpass Filter (LPF), as shown in Figure 3.5, can be expressed as

$$H(j\omega) = \frac{v_o}{v_i} = \frac{1}{1 + j\omega RC} \quad (3.15)$$

By replacing  $j\omega$  by  $j\omega + \sigma = s$  one can express the transfer function as

$$H(s) = \frac{\mathcal{L}\{V_o(t)\}}{\mathcal{L}\{V_i(t)\}} = \frac{1}{1 + sRC} \quad (3.16)$$

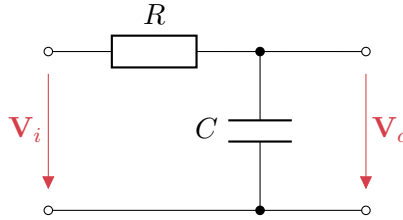


**Figure 3.5:** Simplest passive LPF of first-order

This is the ratio between the Laplace transformed time-domain signals of the output and input respectively. We then generalize the result by normalizing the complex frequency variable  $s$  by defining

$$s_n = \frac{s}{\omega_c} \quad (3.17)$$

For further simplification one can set  $\sigma$  to zero; which is equivalent to assuming sinusoidal form of the input signal. Thus, for  $\sigma = 0$

$$s_n = \frac{j\omega}{\omega_c} = j\frac{f}{f_c} = j\omega_n \quad (3.18)$$

The cutoff frequency of the circuit in Figure 3.5 is  $f_c = 1/(2\pi RC)$ . By definition the normalized complex frequency variable thus becomes  $s_n = 2\pi RC$ . Therefore, the transfer function can be written as

$$H(s_n) = \frac{1}{1 + s_n} \quad (3.19)$$

The magnitude  $|\mathbf{H}(j\omega_n)|$  and phase  $\varphi = \angle \mathbf{H}(j\omega_n)$  of the transfer function for sinusoidal signals are then given by

$$|\mathbf{H}(j\omega_n)|^2 = \frac{1}{1 + \omega_n^2} \quad \text{and} \quad \varphi = \angle \mathbf{H}(j\omega_n) = \arctan \frac{1}{1 + j\omega_n} \quad (3.20)$$

For frequencies  $\omega_n \gg 1$  one can approximate  $|\mathbf{H}| = 1/\omega_n$ . This corresponds to a reduction in gain of 20 dB per frequency decade.

If a sharper cutoff is required,  $N$  LPFs can be connected in series. The Transfer Function (TF) then becomes

$$\mathbf{H}(s_n) = \prod_{i=1}^N \frac{1}{1 + \alpha_i s_n} \quad (3.21)$$

where  $\alpha_i$  are real and positive coefficients and for frequencies  $\omega_n \gg 1$ ,  $|\mathbf{H}| \approx 1/\omega_n^N \propto 1/\omega^N$ . The gain therefore falls off at  $N \cdot 20$  dB per decade. It can be observed that the TF possesses  $N$  real and negative poles. This is characteristic of  $N$ th-order passive  $RC$  LPF.

If we cascade LPFs with identical cutoff frequencies, then

$$\alpha = \alpha_i = \sqrt{\sqrt[N]{2} - 1} \quad (3.22)$$

which is the condition for which *critical damping* occurs. Each individual cutoff frequency is a factor  $1/\alpha$  higher than that of the filter as a whole.

The TF of the  $N$ th-order LPF has the general form

$$H(s_n) = H_0 \left( 1 + \sum_{i=1}^N c_i s_n \right)^{-1} \quad (3.23)$$

where  $c_i$  are real and positive coefficients and the order of the filter is equal to the highest power of  $s_n$ . By rewriting the denominator in factored form and allowing complex poles, one denotes Equation 3.23 as

$$H(s_n) = \frac{H_0}{(1 + a_1 s_n + b_1 s_n^2)(1 + a_2 s_n + b_2 s_n^2) \cdots} \quad (3.24)$$

where  $a_i$  and  $b_i$  are real and positive coefficients and  $b_1 = 0$  for odd orders  $N$ .

The frequency response can be optimized to different theoretical aspects by setting the coefficients  $a_i$  and  $b_i$ . As a consequence of these optimizations, complex poles arise, that cannot be realized by blocks of passive  $RC$  filters. It is possible to meet the optimized conditions by using  $LRC$  filters with the simplest example shown in Figure 3.6, where

$$H(s) = \frac{1/(LC)}{s^2 + \frac{R}{L}s + \frac{1}{LC}} \quad \text{and} \quad f_c = \frac{1}{2\pi\sqrt{LC}} \quad (3.25)$$

This design does not pose any difficulties when opting for high cutoff frequencies. But it is apparent, that one requires the use of large capacitances as well as large inductances for low cutoff frequencies. And because large inductances are unwieldy and have poor electrical properties, an active filter design is better suited for low cutoff frequencies. With these designs the use of inductances are avoided by the addition of active elements, namely OPAs, to the  $RC$  network.

### 3.3 Filtering

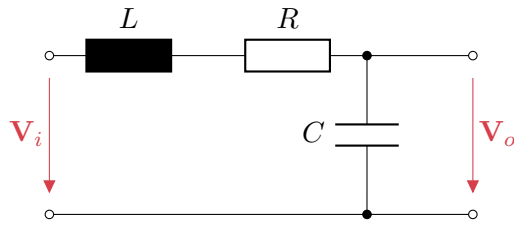


**Figure 3.6:** Passive second-order LPF, LRC circuit

#### 3.3.2 Optimization of Lowpass Filters

We take the *standard form* of the second-order LPF into consideration, where:

$$H(s_n) = \frac{H_0}{1 + a_1 s_n + b_1 s_n^2} = \frac{k}{1 + \frac{s_n}{Q} + s_n^2} = \frac{k}{1 + 2\zeta s_n + s_n^2} \quad (3.26)$$

$$Q = \frac{1}{2\zeta} = \frac{b_1}{a_1} \quad (3.27)$$

where  $k$  is the gain factor and  $Q$  is the quality factor respectively  $\zeta$  the damping ratio. In the case of unity gain,  $k = 1$ , one can see that the two poles are given by:

$$p_{1,2} = (-\zeta \pm \sqrt{\zeta^2 - 1})\omega_n \quad (3.28)$$

and that the poles are...

- real if  $\zeta \geq 1$
- complex if  $0 < \zeta < 1$
- imaginary if  $\zeta = 0$
- in the right half plane and unstable with  $\text{Re}\{p\} > 0$  if  $\zeta < 0$

If we now take a look at the second-order system used to describe the accelerometer dynamics in (2.2) and replace the static sensitivity  $K$  with the gain factor  $k$  the system dynamics are equal and one can see the influence of the damping factor on the system behavior in Figure 2.4. Many filter designs expose this configurability of a second order systems. Because of parameters  $k$  and  $\zeta$  respectively  $Q$  to tune the filter behavior and gain different optimization points targeted. Moreover, when connecting multiple second-order filters in series to realize higher-order filters with steeper roll-offs, the individual second-order filter parameters can be tuned to match three distinct optimization points:

- The *Chebyshev* filter is optimized to have a steep roll-off rate but shows ripple in the pass- and stopband.
- The *Butterworth* filter is optimized to have the most stable gain at the passband but has a poor roll-off rate.
- The *Bessel* filter is optimized to have the most stable phase response, which is critical for fast signal level changes. The caveat comes in form of the poorest roll-off of all filters, when compared at same order.

Here the bandpass refer to the until gain section in the filter up until the cutoff frequency and the stopband is defined depending on application. If one expects high noise densities directly above the cutoff frequency,

the stop band needs to be defined at a low gain and the roll-off of the filter must designs to be steep, whereas if some application only allows small phase shifts, the latter cannot be achieved by a high order filter. The definition of the cutoff frequency is more consistent. For most filters the cut-off frequency is reached, when the gain reaches  $-3$  dB, i.e. approximately when the filter halves squared gain, that is proportional to the power transmission. An exception is the Chebyshev here it is common to define the cutoff the point where the filter roll-off reaches minus the maximally allowed ripple gain in decibel, see Figure 3.7. Note that given the three optima, any hybrid filter design between the Chebyshev and the Butterworth as well as between the Butterworth and Bessel is possible too.

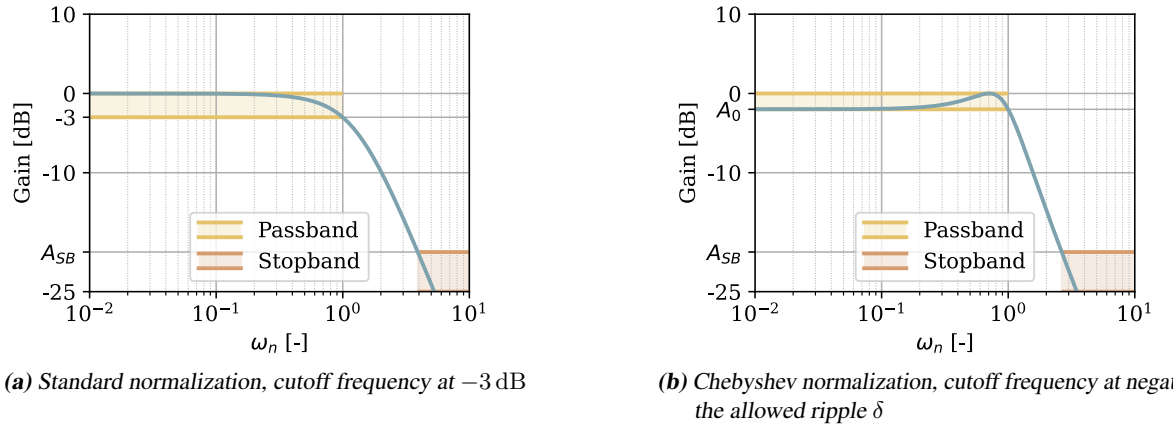


**Figure 3.7:** LPF Pass- and Stopband, where the passband is defined by  $\omega_n < 1$  and the stopband is chosen depending on the application (usually starting at  $-20 \dots -160$  dB)

Until now we described all-pole LPFs, i.e. no nodes are present in the filter system, as can be seen in the TF of (3.24). With filter designs that include nodes, one can realize sharper cutoffs without increasing the phase shift. Generally more complex filter curves are possible at the cost of more unstable behavior and more complex filter design. Due to these disadvantages their behavior is not as reliable as the filters listed before. Therefore they were not considered during this thesis. For more background on these filters, also called *elliptic-function* filters, we advice to take look at the textbook [16] for more background.

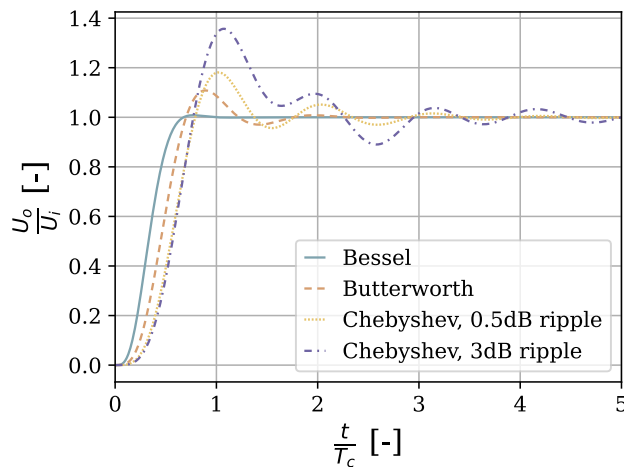


**Figure 3.8:** Step response of fourth-order LPF — Note, that the Chebyshev filter is represented with the cutoff frequency at  $-3$  dB for comparability.

### 3.3 Filtering

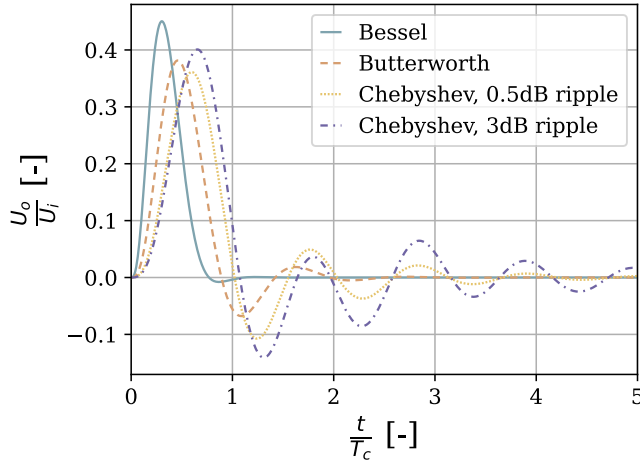


**Figure 3.9:** Impulse response of fourth-order LPF — Note, that the Chebyshev filter is represented with the cutoff frequency at  $-3$  dB for comparability.

## Active Filter Designs

### Chebyshev Lowpass Filter

In the passband the Chebyshev LPF is allowed to have a predetermined ripple. The characteristic of Chebyshev polynomials is, that the ripple ripples are constant, i.e. their local extrema in the gain plot can be connected by two horizontal lines that are displaced by the predetermined ripple.

$$T_N(x) = \begin{cases} \cos(N \arccos x), & \text{for } 0 \leq x \leq 1 \\ \cos(N \operatorname{arccosh} x), & \text{for } x > 1 \end{cases} \quad (3.29)$$

To get the LPF from these Chebyshev polynomials, we define

$$|\mathbf{A}|^2 = \frac{k A_0^2}{1 + \varepsilon^2 T_N^2(x)} \quad (3.30)$$

where  $A_0$  is the so called DC- or zero-gain and the constant  $k$  is chosen such that, for  $x = 0$ , the square of the gain  $|\tilde{\mathbf{A}}|^2$  becomes  $A_0^2$ . If  $N$  is even, that is  $k = 1$  and if  $N$  is odd, we set  $k = 1 + \varepsilon^2$ . The latter is a measure of the ripple and is given by

$$\frac{A_{\max}}{A_{\min}} = \sqrt{1 + \varepsilon^2} \quad (3.31)$$

and

$$\left. \begin{array}{l} A_{\max} = A_0 \sqrt{1 + \varepsilon^2} \\ A_{\min} = A_0 \end{array} \right\} \quad \text{if } N \text{ is even} \quad \left. \begin{array}{l} A_{\max} = A_0 \\ A_{\min} = A_0 / \sqrt{1 + \varepsilon'^2} \end{array} \right\} \quad \text{if } N \text{ is odd} \quad (3.32)$$

Once  $|\mathbf{A}|^2$  is determined, the complex gains can be calculated. However, it is easier to derive the poles of the transfer function directly of the Butterworth filters. By combining the complex conjugates the

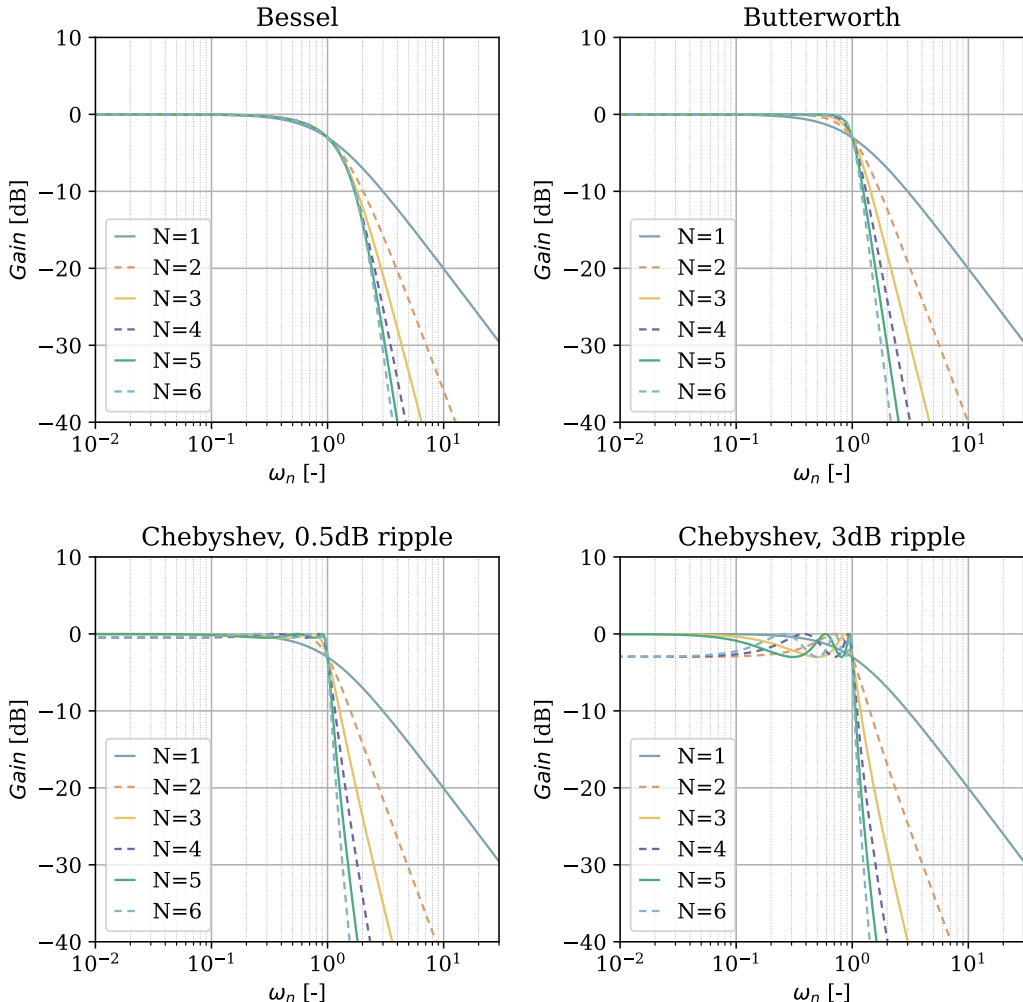


**Figure 3.10:** Influence of LPF order  $N$  on the amplitude of the frequency response — Note, that the Chebyshev filter is represented with the cutoff frequency at  $-3$  dB for comparability.

coefficients  $a_i$  and  $b_i$  in (3.24) are determined:

$$\left. \begin{array}{l} b'_i = \frac{1}{\cosh^2 \gamma - \cos^2 \frac{(2i-1)\pi}{2N}} \\ a'_i = 2b'_i \cdot \sinh \gamma \cdot \cos \frac{(2i-1)\pi}{2N} \\ b'_1 = 0 \\ a'_1 = 1/\sin \gamma \\ b'_i = \frac{1}{\cosh^2 \gamma - \cos^2 \frac{(i-1)\pi}{N}} \\ a'_i = 2b'_i \cdot \sinh \gamma \cdot \cos \frac{(i-1)\pi}{N} \end{array} \right\} \begin{array}{l} \text{if } N \text{ is even and} \\ \text{for } i = 1 \dots \frac{N}{2} \\ \text{if } N \text{ is odd and} \\ \text{for } i = 2 \dots \frac{N+1}{2} \end{array}$$

where  $\gamma = \frac{1}{N} \operatorname{arcsinh} \frac{1}{\varepsilon}$

### 3.3 Filtering

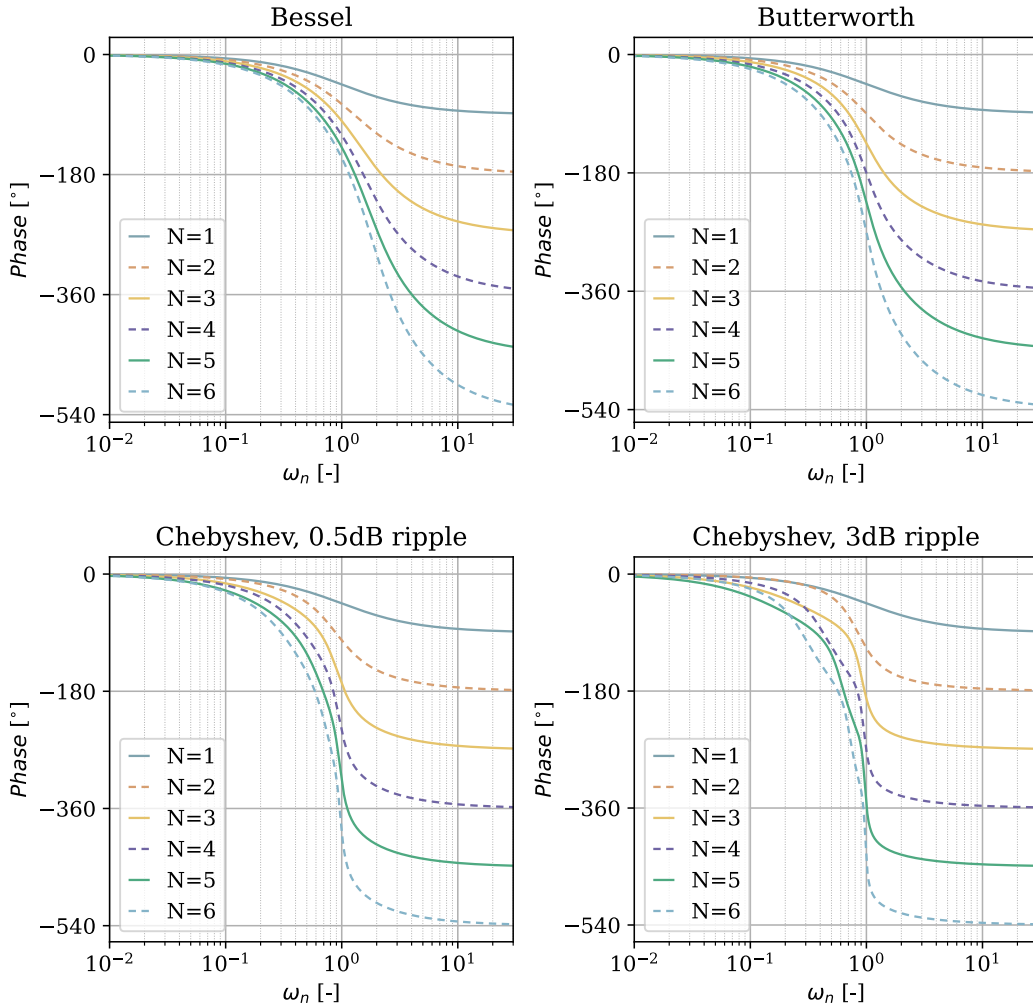


**Figure 3.11:** Influence of the LPF order  $N$  on the phase of the frequency response — Note, that the Chebyshev filter is represented with the cutoff frequency at  $-3$  dB for comparability.

The obtained coefficients  $a'_i$  and  $b'_i$  define a Chebyshev filter at the cutoff frequency  $\omega_x$ , which the gain assumes the value  $A_{\min}$  for the last time. For easy comparison with other filter types we want to evaluate the filter at a cutoff frequency where the gain is  $-3$  dB. For this we multiply the normalized frequency  $s_n$  with a real constant  $\alpha$ , changing the quadratic expressions in the denominator of (3.24) to

$$(1 + a'_i \alpha s_n + b'_i \alpha^2 s_n^2) \quad (3.33)$$

Next, we evaluate  $\alpha$ , so that the gain value is  $1/\sqrt{2} - 3$  dB at the normalized frequency  $s_n = j$ . The coefficients for the filter with cutoff frequency pass through at  $-3$  dB can then be determined by multiplication with the constant.

$$a_i = \alpha a'_i \quad \text{and} \quad b_i = \alpha^2 b'_i$$

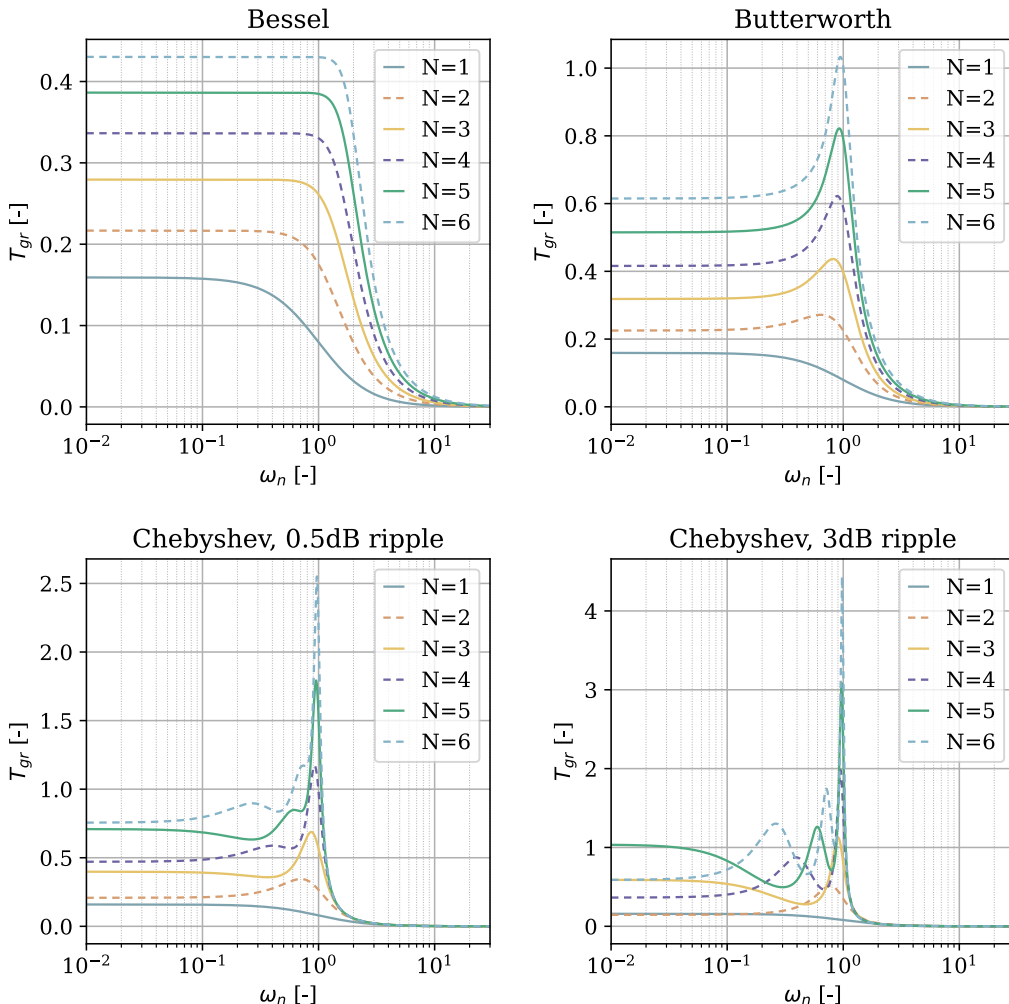


**Figure 3.12:** Influence of the LPF order  $N$  on the group delay of the frequency response — Note, that the Chebyshev filter is represented with the cutoff frequency at  $-3$  dB for comparability.

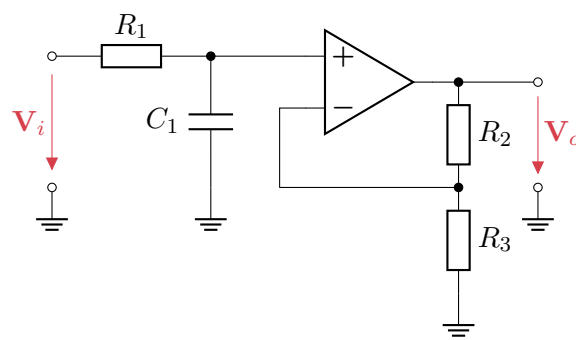


**Figure 3.13:** Active first-order LPF with impedance converter

### 3.3 Filtering

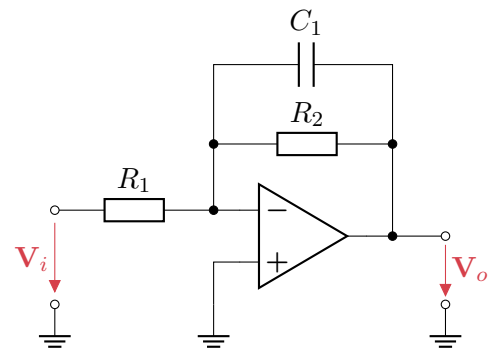


**Figure 3.14:** Active first-order LPF with inverting amplifier

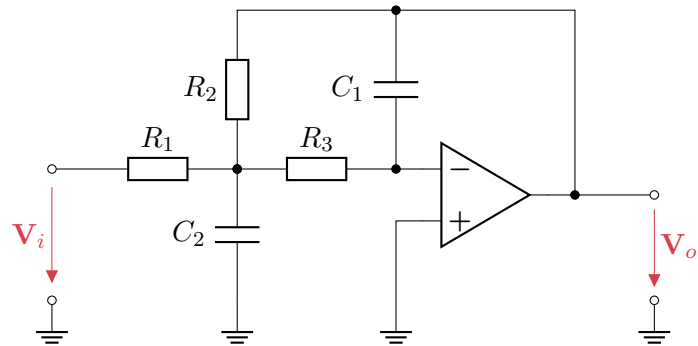


**Figure 3.15:** Active second-order LPF with multiple negative feedback

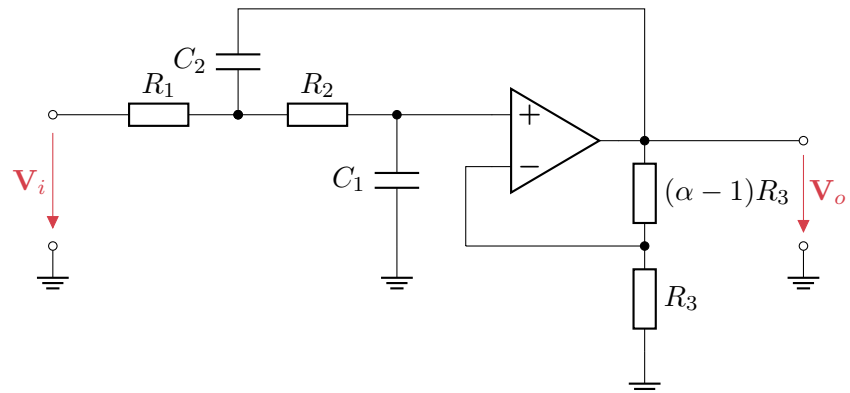


**Figure 3.16:** Active second-order LPF with single positive feedback

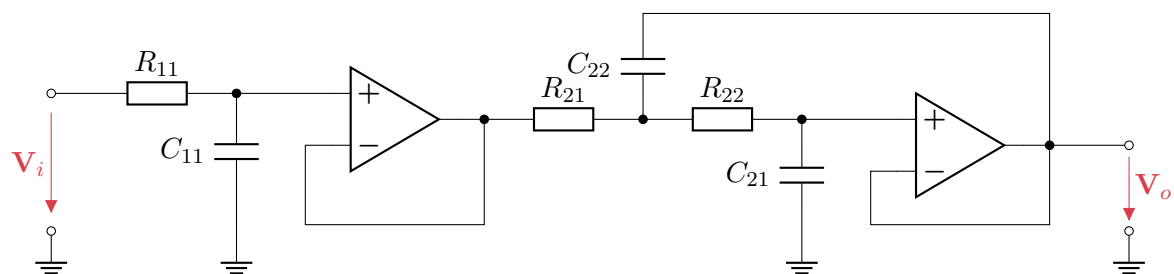


**Figure 3.17:** Active third-order LPF

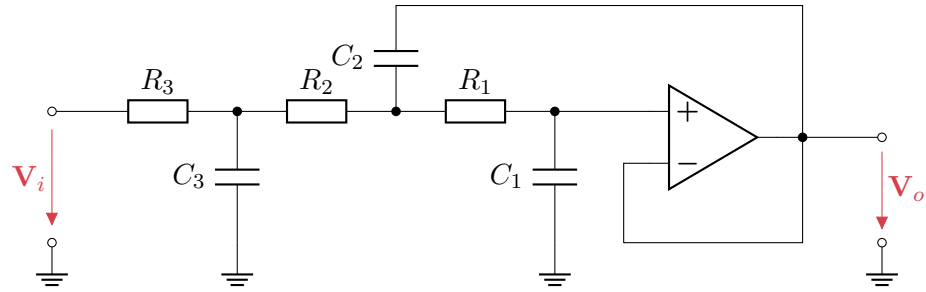


Figure 3.18: Simplified active third-order LPF

In

### Butterworth Lowpass Filter

From the general solution in Equation 3.23 the squared absolute gain in LPFs takes the form

$$|\mathbf{H}(\omega_n)|^2 = H_0^2 \left( 1 + \sum_{i=1}^N k_{2i} \omega_n^{2i} \right)^{-1} \quad (3.34)$$

where odd powers of  $\omega_n$  do not occur, since  $|\mathbf{H}|^2$  must be an even function. In Butterworth LPFs the function  $|\mathbf{H}|^2$  must be maximally flat at  $\omega_n < 1$ , i.e. for frequencies below the cutoff frequency. This condition is best met if we only keep the highest order term, since lower order terms contribute the most to the denominator at low frequencies, decreasing the gain. Hence, for Butterworth LPFs

$$|\mathbf{H}(\omega_n)|^2 = \frac{H_0^2}{1 + k_{2N} \omega_n^{2N}} \quad (3.35)$$

where  $k_{2N} = 1$  due to the normalizing condition, which states that the square of the gain is reduced by 3 dB at  $\omega_n = 1$ , i.e.  $|\mathbf{H}(\omega_n = 1)|^2 \approx |\mathbf{H}(\omega_n = 0)|^2/2$ .

When implementing a Butterworth LPF, one needs to consider the complex gain  $\mathbf{H}$  involved in Equation 3.34. It can be determined by solving for coefficients  $c_i$  in Equation 3.23, given the squared gain of Equation 3.34. It is then possible to solve the transfer function analytically by combining complex conjugate poles. In the solution, we obtain the coefficients  $a_i$  and  $b_i$  of the quadratic expression in Equation 3.24

even order  $N$ :

$$a_i = 2 \cos \frac{(2i-1)\pi}{2N} \quad \text{for } i = 1, 2, \dots, \frac{N}{2} \quad (3.36)$$

$$b_i = 1 \quad (3.37)$$

odd order  $N$ :

$$a_2 = 1, \quad a_i = 2 \cos \frac{(i-1)\pi}{N} \quad \text{for } i = 2, 3, \dots, \frac{N+1}{2} \quad (3.38)$$

$$b_1 = 0, \quad b_i = 1 \quad (3.39)$$

## Bessel Lowpass Filter

### 3.3.3 Anti Aliasing Filter

The Anti Aliasing Filter (AAF) is used ahead of ADCs to reduce the signal bandwidth. More precisely, it aims to reduce the aliasing effect, i.e. the artificial distortion of signals, that occurs when sampling at a finite frequency.

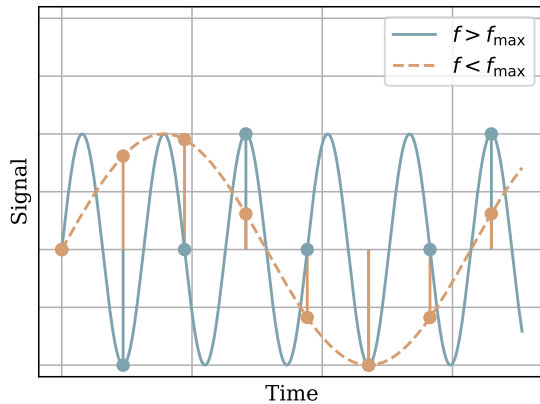


**Figure 3.19:** Aliasing effect

## 3.4 Analog to Digital Conversion

Additionally to other noise sources in the signal chain the ADC shows internal noise that can categorized into two uncorrelated main sources. The quantization noise and the thermal noise. The total internal noise can thus be expressed as the Euclidean norm of these two sources.

$$n_{\text{ADC}} = \sqrt{n_{\text{ADC, Thermal}}^2 + n_{\text{ADC, Quantization}}^2} \quad (3.40)$$

Quantization noise is present due to the process of mapping an infinite number of possible electrical signal values in an analog signal to a finite number of digital codes. Subsequently, any digital output corresponds to an infinite number of analog inputs within range of the output value, plus and minus half the Least Significant Bit (LSB) size,  $s_{\text{LBS}}$ . One can decrease quantization noise by choosing a higher resolution ADC.

$$s_{\text{LBS}} = \frac{V_{\text{FSR}}}{2^m} \quad (3.41)$$

where

$V_{\text{FSR}}$  is the full-scale range of the analog input value and  
 $m$  is the resolution in number of bits

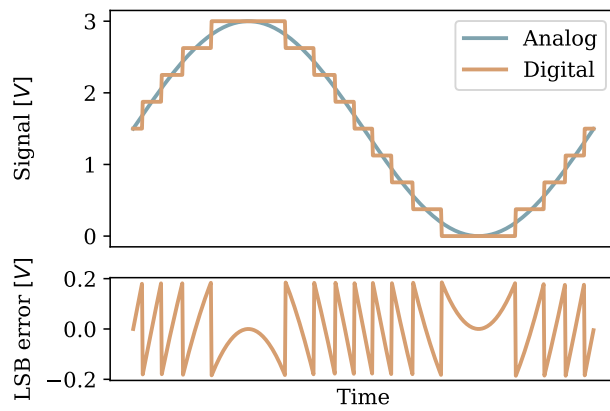


**Figure 3.20:** ADC — Analog input, digital output and LSB error waveform with  $s_{LBS} = 375 \text{ mV}$  [6]

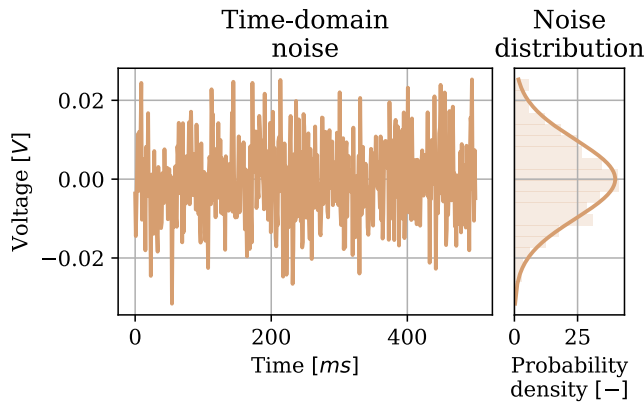


**Figure 3.21:** ADC — Thermal noise in the time domain with Gaussian probability density [6]

Thermal noise is a phenomenon inherent in all electrical components. Because of this, it is a function of the device design and cannot be affected by the embedded system designer. Typically, one assumes the thermal noise to have a Gaussian distribution.



# 4

## Data Acquisition and Software

### 4.1 Data acquisition

The DAC system developed in this thesis is an open source Arduino based system consisting of multiple microcontrollers. All signal channels are transmitted to a central microcontroller before passing to a computer that serves as visualization and analysis tool.

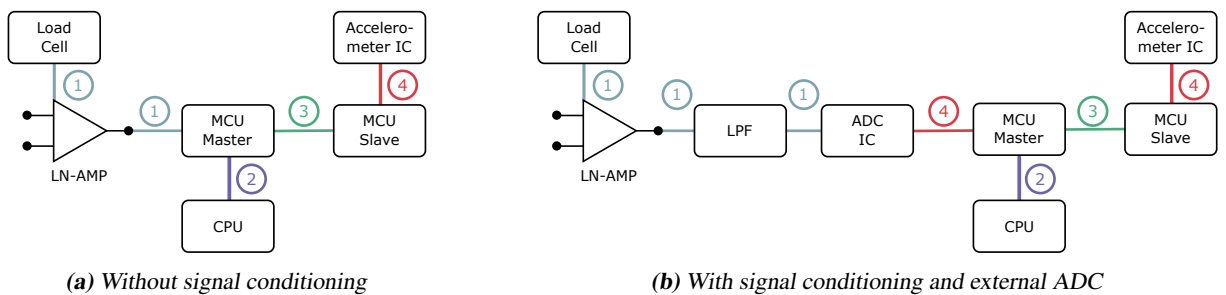


**Figure 4.1:** DAC-system building blocks — note that 4.1a has been realized, but 4.1b has not been implemented yet, due to communication issues between the devices

#### 4.1.1 Building Blocks

Building blocks are the main components used in the DAC signal chain. Additional components that are required to enable the stable operation of the building blocks are not listed.

Because of the accelerometer IC output interfaces it is not possible to connect all sensors directly to one MCU that acts as a DAC. We need to transform the signal to a different interface. A low-cost and versatile method to achieve this, is to use a MCU for each accelerometer IC. These read the sensor IC registers and

## 4.1 Data acquistion

Interfaces
<span style="color: #008080; border: 1px solid black; border-radius: 50%; padding: 2px;">1</span> : Analog Signal
<span style="color: #800080; border: 1px solid black; border-radius: 50%; padding: 2px;">2</span> : USB
<span style="color: #008000; border: 1px solid black; border-radius: 50%; padding: 2px;">3</span> : RS-485
<span style="color: #FF0000; border: 1px solid black; border-radius: 50%; padding: 2px;">4</span> : SPI

**Table 4.1:** Legend to Figure 4.1

communicate to the MCU master. The master, on the other hand, acts as a passthrough and transmits the data to the Central Processing Unit (CPU). In the setup used, it also reads out the LC signal. Table 4.2 lists the MCUs used during this thesis.

The analog signal output of the LC needs to be amplified to match the input range of the ADC. To gain the maximum resolution, this depends on the expected input range. To get a higher value resolution than offered by the MCU embedded ADC one can set in an external ADC IC upstream to the MCU. Additionally, we use a LPF in Figure 4.1b. The LPF is needed to cut off high frequency components of the signal that occur particularly in sharp impulse signals. This design choice may lead to problems because it is not standard procedure in the development a measurement instrument. Typically, components in the analog signal chain are chosen, based on the frequency bandwidth of the input signal. This means, the cut-off frequency of the LPF is set well above the signal's bandwidth. But because we use low-cost components in our system, the bandwidth is limited to half the sampling rate of the slowest sensor. According to the Nyquist frequency theorem, the cut-off frequency then needs to be reduced to half the sampling frequency, potentially reducing the output magnitude of higher frequency components of the signal.

Name	Core	ADC-Resolution / bit	Operating Voltage / V	Clock Speed / MHz	Flash Memory / kByte	SRAM / k Byte
Arduino Due	AT91SAM3 ARM Cortex	12	3.3	84	512	96
Teensy 3.2	MK20DX256VLH Cortex-M4	13 (16 bit-values)	3.3	72	256	64
Robotdyn Blackpill	STM32F103C8 Cortex-M3	12	72	64	20	

**Table 4.2:** List of MCUs used in this work

Instrumental-Amplifier AD627BRZ

Lowpass Filter LTC1069-1IS8, 8th order, monolithic, clock tunable LTC1154CN, highly customizable filter block LTC1066-1, 8th order, clock tunable DAC

ADC EVAL-AD7988, evaluation board for SAR-ADC

### 4.1.2 Interfaces

The interfaces are the connections and protocols between the different building blocks of the DAC system. The interfaces are chosen based on the sensors used and the expected data rate at the required cable length

between each section. I.e.:

- Between the analog LC and the external ADC in Figure 4.1b and the MCU integrated ADC in Figure 4.1a respectively the signal transmission is analog.
- The register of the accelerometer IC is accessed via SPI
- The communication between MCUs is rooted in RS-485 differential transmission to accommodate for signal transmission over cable lengths greater than 10 m and uses a specialized protocol to keep data packages as small as possible.
- Between the MCU and the CPU USB transmits data using the serial class of the Arduino software.

Data rates and package sizes are critical when sampling at high frequencies.

With RS-485 data can be transmitted over distances of no less than 100 km at a data rate of 1 kbit/s. At 1200 m cable length we can reach data rates of around 100 kbit/s. In our range of application, i.e. a few tens of m, we can expect data rates of 1 Mbit/s, thus representing the bottle neck in the digital data chain. If we then transmit 80 bit acceleration measurements (see Figure 4.2) at 1.6 kHz we stay below this expected limit by a safety factor of more than 10. The arduino the serial package parses all data as human readable code, specifically American Standard Code For Information Interchange (ASCII). In this format every digit of integer values is passed as 8 bit-value. Which means that a 32 bit timestamp and every single axis acceleration are passed as ten 8 bit-values and six 8 bit-values respectively. This increases the size of an accelerometer package to 624 bit, which in turn reduces the safety factor to approximately 1. It is clear that one cannot use human readable code to transmit the data and guarantee stability at the required sampling rate.

### MCU communication protocol

The communication protocol for MCU to MCU and MCU to computer was developed for this project.

<code>&lt;[ (reg) (#bytes) (data) ]&gt;</code>
<code>&lt;[/&gt;</code> : Start-/End-bytes, represented as ASCII
(reg) : Registry/Address of the transmission
(#Bytes): Number of bytes in transmission
(data) : Data to transmit

**Table 4.3:** Protocol used to communicate between two MCU's and between MCU and computer

#### 4.1.3 Dataflow

The dataflow between the MCUs is sequential and all data is passed to a central MCU, called master, before we streamline it to the CPU. The master cycles through all connected MCU performing a data request, hold and receive action. As soon as a slave MCU gets a request, it transmits a data package from its buffer. The master, now receiving the data package, will throughput the signal to the CPU, where the data is stored. By the end of this process the master will jump to the next slave.

All measurements consist of a 32 bit-timestamp and the measured values and are pushed into a First In, First Out (FIFO) buffer in the flash memory of the MCU, directly connected to the sensor. Bundled data

## 4.2 Software

packages are then pulled from the buffer and translated into the transmission code as defined in Table 4.3. In Figure 4.2 the data flow is represented by a system that is using only one slave MCU, displayed in violet.

Clock synchronizations are executed in form digital data exchange, by synchronizing the timestamps before a complete measurement. The sensor measurements themselves are conducted as soon as ready to benefit of the sensors maximum measurement frequency. With this method, no data bandwidth is used between measurement cycles for clock synchronization, but it comes with three caveats. Firstly, every MCU runs on its own clock cycle. Measurements are conducted whenever the individual time interval after the clock is exceeded. These time intervals are matched by sharing the master timestamp with the ones of the slave programmatically. The slave timestamps are then tuned to same value during a setup process. But after the synchronization the Gaussian distributed deviations to the intervals accumulate, ultimately yielding unknown time-shifts to the signals.

Measurements are packaged due to the time the master requires to change the communication to another slave. During these switches no data is transmitted eventually limiting the data rate of the system.

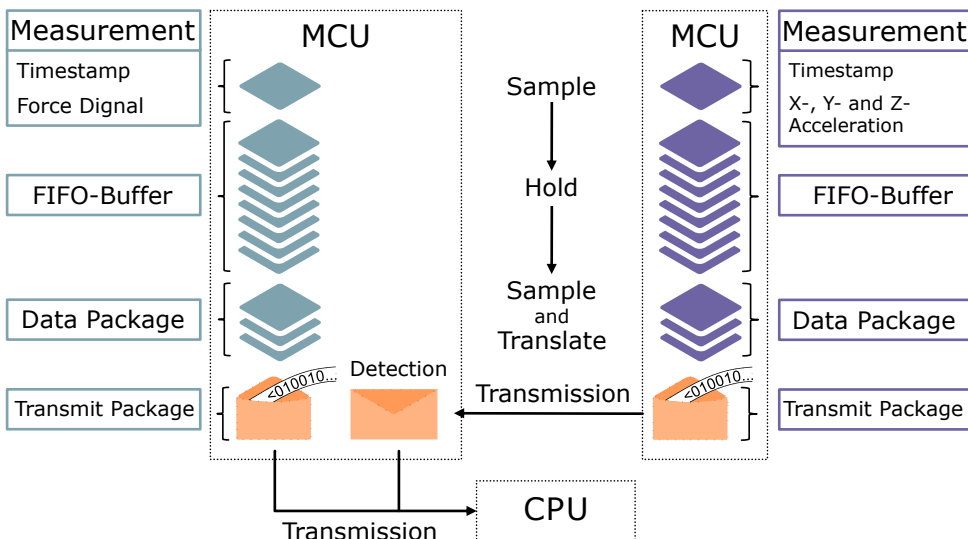


**Figure 4.2:** Data flow between two MCUs and the CPU

## 4.2 Software

The software developed during this project is split into the Arduino software running on the MCUs and a python based tool to receive and visualize the data via USB.

For the instrument to work, some functions are required, while other desired functions are tools that simplify the workflow during measurements and facilitate bug fixes in the software.

The requirements to the software tools are:

- m1 Read out accelerometer and LC data at the maximum sample speed of the accelerometer IC.
- m2 Synchronize measurements timestamps.
- m3 Initialize measurement by hammer impulse.

The desired software tools are:

- $w1$  Generate continuous real time output of measurement data.
- $w2$  Track data transfer via USB.



# 5

## Test Setups

The test conducted during this thesis isolated features of the prototype system described in Chapter 4. Measurement data has been compared to a reference system, called MODE3. Both systems are configured to include one impulse hammer, one DAC system and one three dimensional accelerometer, as well as a read out computer system with accompanying software.

### 5.1 Hammer-Hammer Test

The hammer tips of the impact hammers of both the the prototype system and the MODE3 are hit against each other. The target of this test is to evaluate the signal quality of the LC in the prototype system.

We assume the force transmission from the point of impact to both load cells respectively to be lossless. Thus the recording accuracy of the prototype system is determined by the correlation of the two signal recordings.

The configurations used in the tests are listen in Table 5.1. The components are shown in Figure 5.1. All hammer-hammer tests were conducted, using a DAC of form Figure 4.1a

Sensor Parameter	Reference Hammer	Prototype Hammer
Sampling rate	1600 Hz	1600 Hz
Dynamic Range	0...20 kN	0...3 kN
Quantization resolution	24 bit	12 bit

**Table 5.1:** Hammer-hammer test configuration

## 5.2 Andromeda Measurement

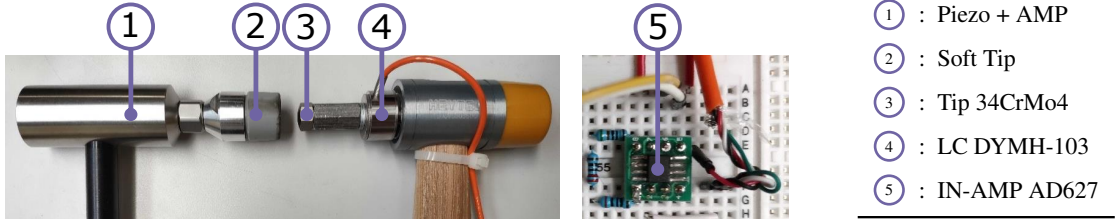


**Figure 5.1:** Hammer-Hammer test components

**Table 5.2:** Legend to Figure 5.1

## 5.2 Andromeda Measurement

In the Andromeda measurement the accelerometers of both systems are positioned at close locations on the Andromeda test bench. Impact hammers of both the prototype and the reference system may be used as input signal. Because of this, the recording of the accelerometer signal of whichever system's impact hammer is not in use, is initiated before the impact and over a longer time frame. To compare signals of both systems, they are synchronized in the post analysis. The target of this test is to evaluate the signal quality of the accelerometer in the prototype system.

The Andromeda test bench consists of a wagon that is supported by a 3 m long linear drive in the x-axis on two 2.6 m apart, gantry y-axes that are linear drives as well. Hence kinematic chain

$$V[b[Y1Y2]X]$$

Figure 5.2 shows the test setup, while Figure 5.3 shows an example position of impact in the test setup.

The focus of this test is to compare the accelerometer signals. Therefore, we set the accelerometer parameter as defined in Table 5.3

Sensor Parameter	Sample Rate / Hz	Dynamic Range / g	Quantization / bit
Reference	1600	$\pm 5$	24
Prototype	1600	$\pm 4$	16

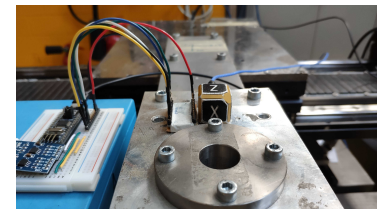
**Table 5.3:** Accelerometer parameter settings

## 5.3 Other Test Setups

To test the bandwidth of the prototype LC the hammer tip is hit against a rigid surface. The hardness of the hammer tip determines the bandwidth of the signal. And with hard tips the highest bandwidths can be explored. Apart from the signal measurement tests themselves other tests had to be conducted to guarantee the DAC operation and to test the Software. As an example, clock tunable LPF are tested in an arduino circuit, that generates a differential sinusoidal signal at different frequencies.

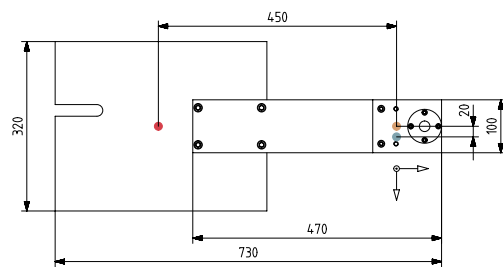


(a) Andromeda test setup

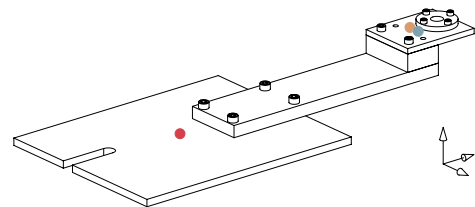


(b) Accelerometer view

**Figure 5.2:** Andromeda test setup



(a) Top view



(b) Trimetric view

**Figure 5.3:** Andromeda wagon, example impact position



# 6

## Results and Discussion

In this chapter the results of the setups in ?? are discussed.

### 6.1 Hammer-Hammer Test

The results of the hammer-hammer test are impulse signal recordings of both, the reference system and the prototype LC. Because the prototype signal is not calibrated, in order to able to compare the signals one needs to normalize the signal range of the reference signal. Furthermore, the signals need to be synced in time, by applying a time shift to one. The outputs gained after these transformations are shown in Figure 6.1.

It can be seen that if one is using the soft PVC tip of the reference system both signals correlate well. If we then focus on the detailed view of such a test, as seen in Figure 6.2, the difference in resolution becomes apparent.

### 6.2 Andromeda Measurement

Before comparing the accelerometer signals of the reference with the ones of the prototype system, one needs to subtract the constant gravitational part from the prototype signals. Additionally, the signals need to be synchronized in the time axis, as can be seen in Figure 6.3.

When we then consider the frequency domain of Figure 6.4 one can see that both signals cover the excited frequency bandwidth of around 250 Hz in a similar manner. The initial deviation at 1 Hz can be explained due to the signal conditioning in the reference system, where lower frequencies are cut-off.

### 6.3 Other Test Setups

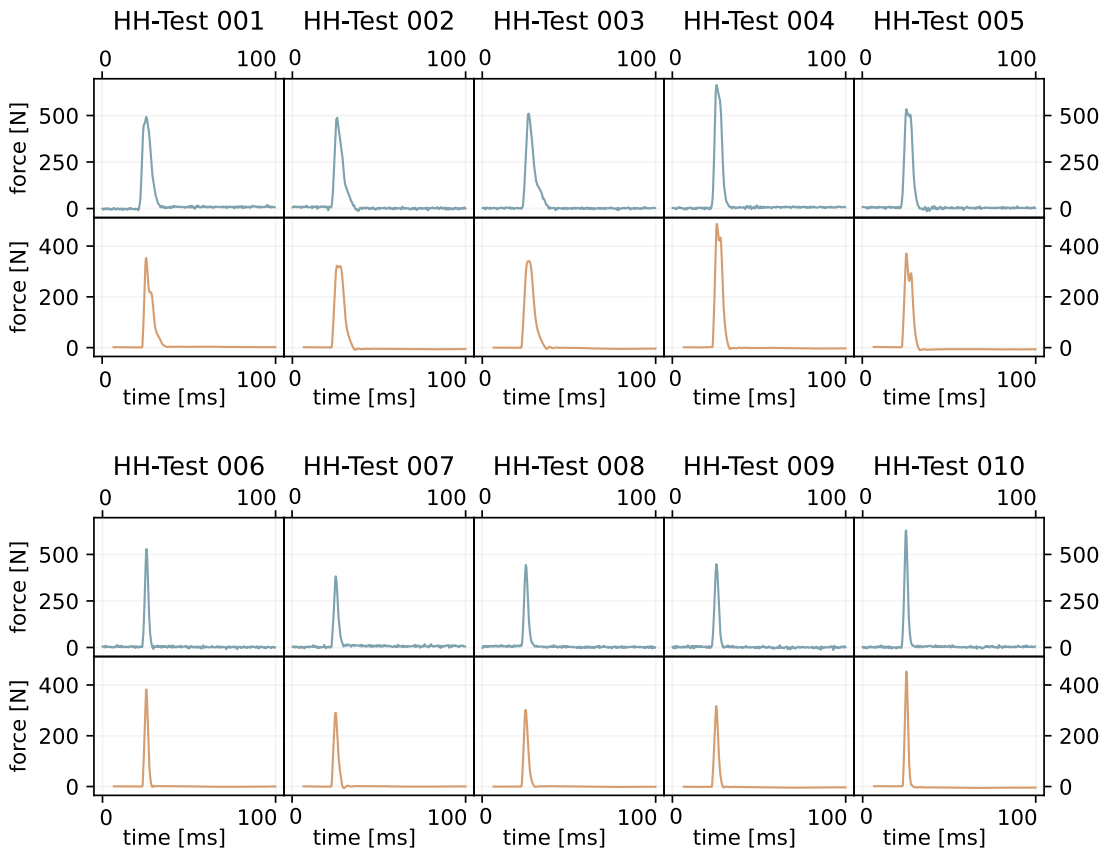


**Figure 6.1:** The HH-Test recordings of the reference hammer (orange) and the evaluated impact hammer system (turquoise). Note that the evaluated signal values are normalized so that the maxima are equal to the reference system.

### HH-Test 006

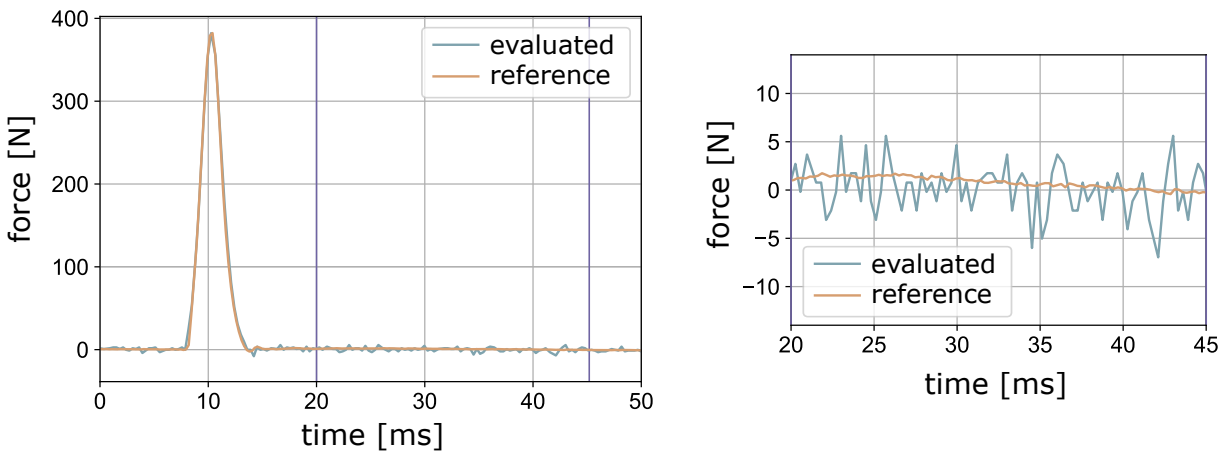


**Figure 6.2:** Detailed plot of HH-Test 006

## 6.3 Other Test Setups

Other tests failed to deliver results:

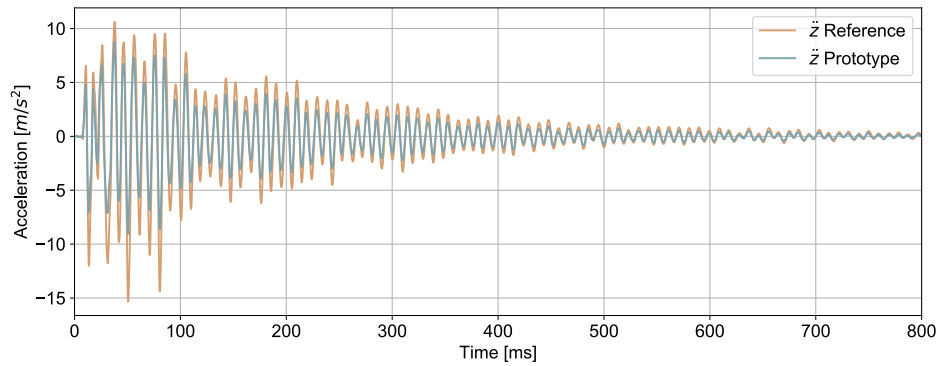


**Figure 6.3:** Measurement HAp024 in the time domain, excitation at point A, as shown in Figure 5.3

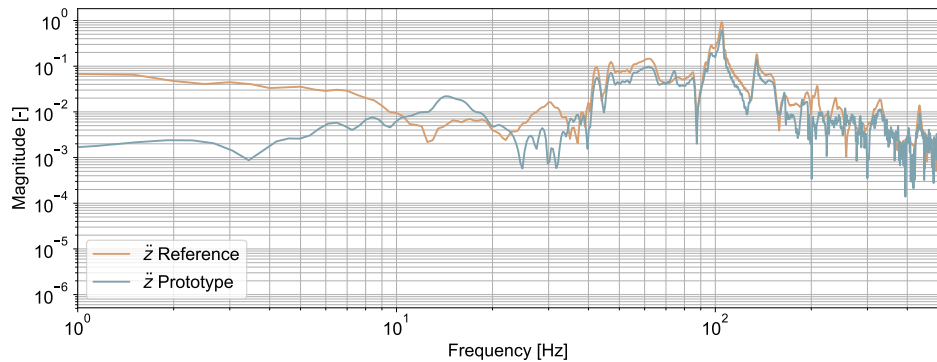


**Figure 6.4:** Measurement FFT HAp024, excitation at point A, as shown in Figure 5.3

- The hammer-surface test did not give insight to the maximum bandwidth of the prototype hammer because of software issues, bottlenecking the data rate.
- The clock tunable filter test failed due to an insufficiently precise clock signal.



# 7

## Conclusion and Future Work

### 7.1 Conclusion

In this thesis

- A low-cost capacitive accelerometer IC has been used to measure the output signal of an EMA measurement setup
- An impulse hammer using a strain gauge load cell has been developed using low-cost components.
- Different conditioning filter circuits have been studied and tested for the impulse hammer signal
- A communication protocol has been developed

#### 7.1.1 Deficiencies

Because of the lack of a thorough state of the art research in the beginning of the project, the solution space of the project has been constricted early on. In this solution space, the data rates and the required compute efficiency of MCUs were not met by the software. Furthermore, the issue of conditioning the analog signal of the LC signal has been addressed at a late stage. Leading to no successful hardware setup with an upstream LPF.

## 7.2 Future Work

There are multiple options to progress from this point. They can be framed in ... directions:

- Explore the same solution space further, i.e. handling the LPF circuit and optimizing the software.
- Change to a different solution space with either standard components using CPUs or Field Programmable Gate Array (FPGA)s, targeting simpler implementation or higher bandwidths
- Exploring the limits of the application and limits current solution without additional preconditioning

Independent of the chosen direction one can progress by

- Testing the limits of multi channelling
- Leaving the prototyping stage and simplify the production
- Exploring wireless communication

# A

## Appendix

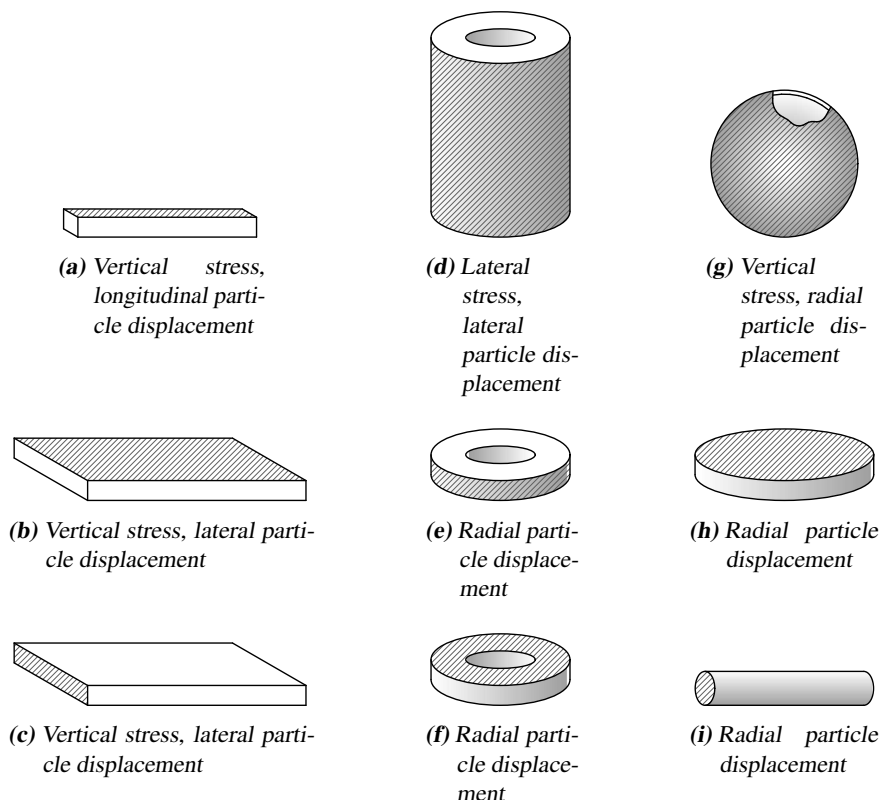


**Figure A.1:** Piezoelectric designs, where electrodes are placed on the shaded areas

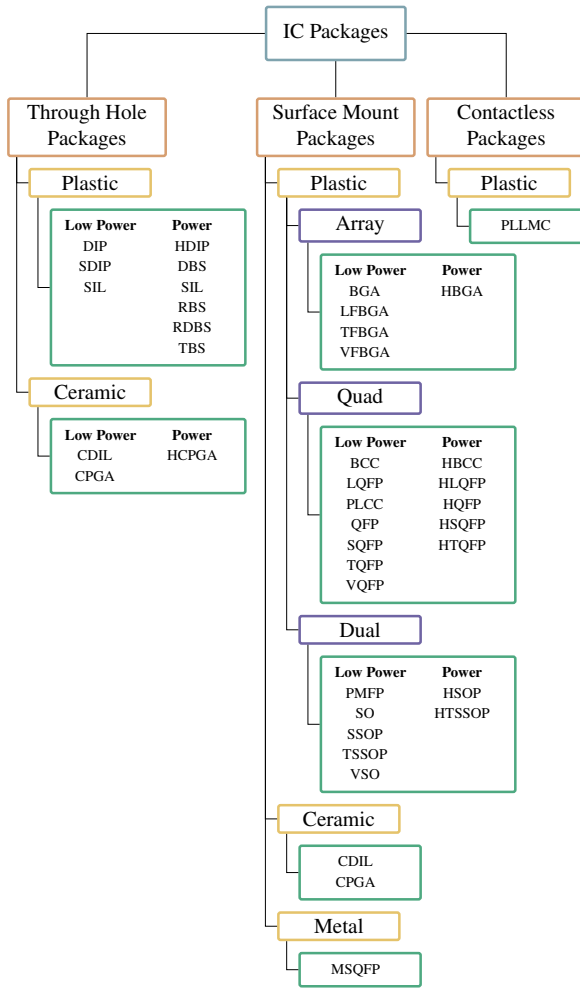


**Figure A.2:** Flowchart of IC packages

**Table A.1:** Andromeda measurement setup that is excited by the prototype impact hammer. The prototype accelerometer is set to a dynamic range of  $\pm 16\text{ g}$  and a AAF cut-off of 800 Hz.

Label	Excitation Location	Prototype Sampling Rate / kHz	Prototype Recording Duration / s
HAe001	A	1.6	3
HAe002	A	1.6	3
HAe003	A	1.6	3
HAe004	A	1.6	3
HAe005	A	1.6	3
HAe006	B	1.6	3
HAe007	B	1.6	3
HAe008	B	1.6	3
HAe009	B	1.6	3
HAe010	B	1.6	3
HAe011	C	1.6	3

continued on next page

**Table A.1:** (Continued)

Label	Excitation Location	Prototype Sampling Rate / kHz	Prototype Recording Duration / s
HAe012	C	1.6	3
HAe013	C	1.6	3
HAe014	C	1.6	3
HAe015	C	1.6	3
HAe016	D	1.6	3
HAe017	D	1.6	3
HAe018	D	1.6	3
HAe019	D	1.6	3
HAe020	D	1.6	3

**Table A.2:** Andromeda measurement setup that is excited by the reference impact hammer

Label	Excitation Location	Accelerometer Sampling Rate / kHz	Prototype Recording Duration / s	Accelerometer Dynamic Range / g	Accelerometer AAF cut-off / Hz
HAp001	A	1.6	3	±16	800
HAp002	A	1.6	3	±16	800
HAp003	A	1.6	3	±16	800
HAp004	A	1.6	3	±16	800
HAp005	A	1.6	3	±16	800
HAp006	B	1.6	3	±16	800
HAp007	B	1.6	3	±16	800
HAp008	B	1.6	3	±16	800
HAp009	B	1.6	3	±16	800
HAp010	B	1.6	3	±16	800
HAp011	C	1.6	3	±16	800
HAp012	C	1.6	3	±16	800
HAp013	C	1.6	3	±16	800
HAp014	C	1.6	3	±16	800
HAp015	C	1.6	3	±16	800
HAp016	D	1.6	3	±16	800
HAp017	D	1.6	3	±16	800
HAp018	D	1.6	3	±16	800
HAp019	D	1.6	3	±16	800
HAp020	D	1.6	3	±16	800
HAp001	A	0.8	3	±16	400
HAp002	A	0.8	3	±16	400
HAp003	A	0.8	3	±16	400
HAp004	A	0.8	3	±16	400
HAp005	A	0.8	3	±16	400
HAp006	B	0.8	3	±16	400

continued on next page

**Table A.2:** (Continued)

Label	Excitation Location	Accelerometer Sampling Rate / kHz	Prototype Recording Duration / s	Accelerometer Dynamic Range / g	Accelerometer AAF cut-off / Hz
HAp007	B	0.8	3	±16	400
HAp008	B	0.8	3	±16	400
HAp009	B	0.8	3	±16	400
HAp010	B	0.8	3	±16	400
HAp011	C	0.8	3	±16	400
HAp012	C	0.8	3	±16	400
HAp013	C	0.8	3	±16	400
HAp014	C	0.8	3	±16	400
HAp015	C	0.8	3	±16	400
HAp016	D	0.8	3	±16	400
HAp017	D	0.8	3	±16	400
HAp018	D	0.8	3	±16	400
HAp019	D	0.8	3	±16	400
HAp020	D	0.8	3	±16	400
HAp021	C	1.6	3	±4	800
HAp022	C	1.6	3	±4	800
HAp023	C	1.6	3	±4	800
HAp024	C	1.6	3	±4	800
HAp025	C	1.6	3	±4	800
HAp026	D	1.6	3	±2	800
HAp027	D	1.6	3	±2	800
HAp028	D	1.6	3	±4	800
HAp029	D	1.6	3	±4	800
HAp030	D	1.6	3	±4	800

**Table A.3:** Hammer-hammer test measurements

Label	Prototype tip	Prototype Sampling Rate / kHz	Prototype Recording Duration / s
HH001	34CrMo4	3	4
HH002	34CrMo4	3	4
HH003	34CrMo4	3	4
HH004	34CrMo4	3	4
HH005	34CrMo4	3	4
HH006	34CrMo4	3	4
HH007	34CrMo4	3	4
HH008	34CrMo4	3	4
HH009	34CrMo4	3	4
HH010	34CrMo4	3	4
HH011	34CrMo4	3	3

continued on next page

**Table A.3: (Continued)**

Label	Prototype tip	Prototype Sampling Rate / kHz	Prototype Recording Duration / s
HH012	34CrMo4	2	3
HH013	34CrMo4	2	3
HH014	34CrMo4	2	3
HH015	34CrMo4	2	3
HH016	Elastomer	2	3
HH017	Elastomer	2	3
HH018	Elastomer	2	3
HH019	Elastomer	2	3
HH020	Elastomer	2	3

**Table A.4: Hammer-surface measurements**

Label	Prototype tip	Prototype Sampling Rate / kHz	Prototype Recording Duration / s
HS001	34CrMo4	2	1
HS002	34CrMo4	2	1
HS003	34CrMo4	2	1
HS004	34CrMo4	2	1
HS005	34CrMo4	2	1
HS006	34CrMo4	2.5	1
HS007	34CrMo4	2.5	1
HS008	34CrMo4	2.5	1
HS009	34CrMo4	2.5	1
HS010	34CrMo4	2.5	1
HS011	34CrMo4	1.67	1
HS012	34CrMo4	1.67	1
HS013	34CrMo4	1.67	1
HS014	34CrMo4	1.67	1
HS015	34CrMo4	1.67	1
HS016	Elastomer	1.67	1
HS017	Elastomer	1.67	1
HS018	Elastomer	1.67	1
HS019	Elastomer	1.67	1
HS020	Elastomer	1.67	1
HS021	Elastomer	2	1
HS022	Elastomer	2	1
HS023	Elastomer	2	1
HS024	Elastomer	2	1
HS025	Elastomer	2	1
HS026	Elastomer	2.5	1

continued on next page

**Table A.4: (Continued)**

Label	Prototype tip	Prototype Sampling Rate / kHz	Prototype Recording Duration / s
HS027	Elastomer	2.5	1
HS028	Elastomer	2.5	1
HS029	Elastomer	2.5	1
HS030	Elastomer	2.5	1

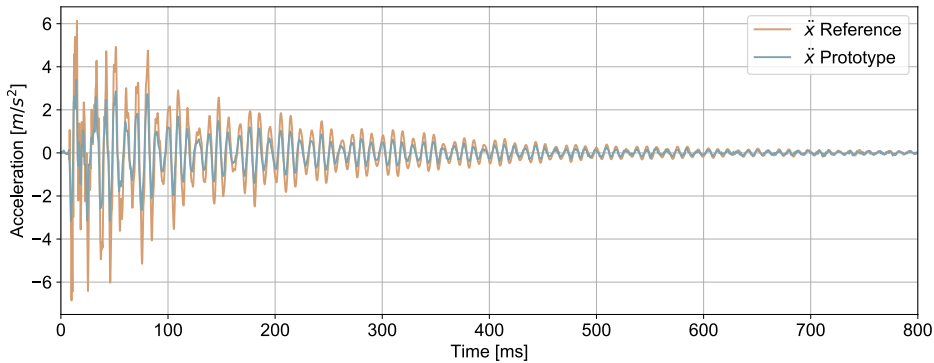


**Figure A.3:** Measurement HAp024 in the time domain, excitation at point A, as shown in Figure 5.3

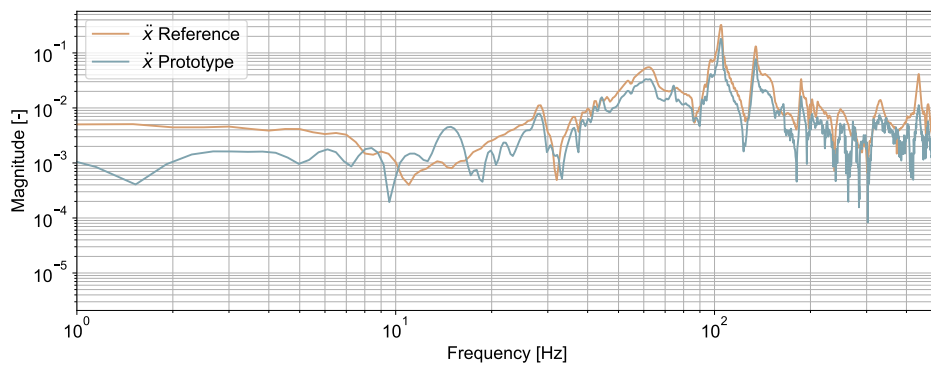


**Figure A.4:** Measurement FFT HAp024, excitation at point A, as shown in Figure 5.3

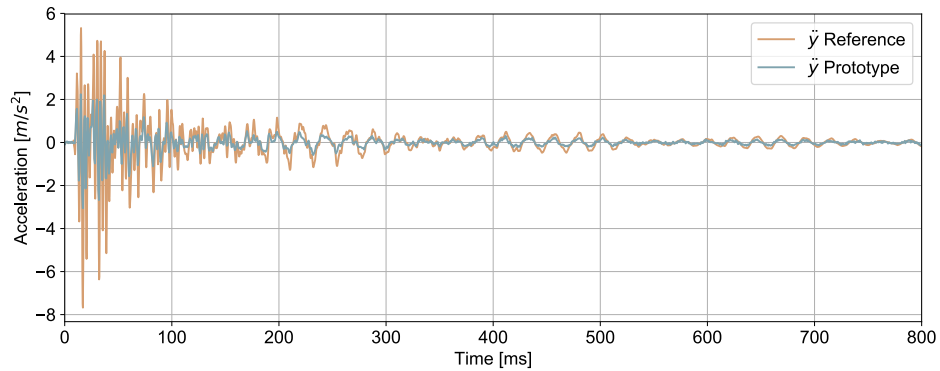


**Figure A.5:** Measurement HAp024 in the time domain, excitation at point A, as shown in Figure 5.3

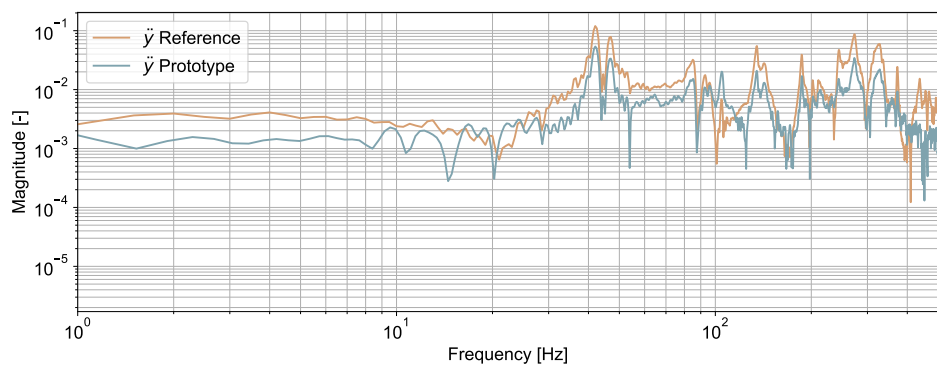


**Figure A.6:** Measurement FFT HAp024, excitation at point A, as shown in Figure 5.3



# List of Figures

2.1	Digital instrument . . . . .	3
2.2	Strain Gauge . . . . .	5
2.3	Piezoelectric accelerometer . . . . .	5
2.4	Second-Order System Bode plots . . . . .	6
2.5	Piezoelectric sensors in amplifier circuits . . . . .	7
2.6	Capacitive displacement sensors . . . . .	9
2.7	Capacitive MEMS Accelerometer . . . . .	9
2.8	Forced Vibration Sources . . . . .	11
2.9	Frequency Response Measurement . . . . .	12
2.10	OSI Model . . . . .	14
3.1	Main OPA types . . . . .	16
3.2	Transfer characteristics of OPAs . . . . .	17
3.3	OPA controllability . . . . .	17
3.4	Equivalent Noise Bandwidth of an Amplifier . . . . .	19
3.5	Passive first-order LPF . . . . .	20
3.6	Passive second-order LPF . . . . .	22
3.7	LPF Pass- and Stopband . . . . .	23
3.8	Step response of fourth-order LPF . . . . .	23
3.9	Impulse response of fourth-order LPF . . . . .	24
3.10	Influence of LPF order $N$ on the amplitude of the frequency response . . . . .	25
3.11	Influence of the LPF order $N$ on the phase of the frequency response . . . . .	26
3.12	Influence of the LPF order $N$ on the group delay of the frequency response . . . . .	27
3.13	Active first-order LPF with impedance converter . . . . .	27
3.14	Active first-order LPF with inverting amplifier . . . . .	28
3.15	Active second-order LPF with multiple negative feedback . . . . .	28
3.16	Active second-order LPF with single positive feedback . . . . .	28
3.17	Active third-order LPF . . . . .	28
3.18	Simplified active third-order LPF . . . . .	29
3.19	Aliasing . . . . .	30

## *List of Figures*

3.20 ADC LSB waveform . . . . .	31
3.21 ADC thermal noise . . . . .	31
4.1 DAC building blocks . . . . .	33
4.2 Data flow . . . . .	36
5.1 Hammer-Hammer Test components . . . . .	40
5.2 Andromeda Test Setup . . . . .	41
5.3 Andromeda Example Positions . . . . .	41
6.1 HH-Test comparison . . . . .	44
6.2 HH006 Plot . . . . .	44
6.3 Andromeda Measurement HAp024, Time Domain in Z-Axis . . . . .	45
6.4 Andromeda Measurement HAp024, FFT in Z-Axis . . . . .	45
A.1 Piezoelectric designs . . . . .	49
A.2 IC packages flowchart . . . . .	50
A.3 Andromeda Measurement HAp024, Time Domain in X-Axis . . . . .	54
A.4 Andromeda Measurement HAp024, FFT in X-Axis . . . . .	54
A.5 Andromeda Measurement HAp024, Time Domain in Y-Axis . . . . .	55
A.6 Andromeda Measurement HAp024, FFT in Y-Axis . . . . .	55

# List of Tables

2.1	Legend to piezoelectric accelerometer . . . . .	5
4.1	Legend to DAC building blocks . . . . .	34
4.2	MCUs used . . . . .	34
4.3	MCU communication protocol . . . . .	35
5.1	Hammer-Hammer Test Configuration . . . . .	39
5.2	Legend to Hammer Hammer Test Components . . . . .	40
5.3	Set Accelerometer Parameters . . . . .	40
A.1	Andromeda Measurements, Prototype Impact Hammer . . . . .	50
A.2	Andromeda Measurements, Reference Impact Hammer . . . . .	51
A.3	Hammer-Hammer Test Measurements . . . . .	52
A.4	Hammer-Surface Measurements . . . . .	53



# Bibliography

- [1] Sherif Beskyroun and Q. Ma. “Low-cost accelerometers for experimental modal analysis”. In: *Proc. of the 15th World Conference on Earthquake Engineering*. 2012.
- [2] Bill Buchanan. *The Handbook of Data Communications and Networks: Volume 2*. Vol. 2. Springer Science & Business Media, 2004.
- [3] Yum Ji Chan and Jing-Wei Huang. “Multiple-point vibration testing with micro-electromechanical accelerometers and micro-controller unit”. In: *Mechatronics* 44 (2017), pp. 84–93.
- [4] Ozak O Esu et al. “Integration of low-cost consumer electronics for in-situ condition monitoring of wind turbine blades”. In: (2014).
- [5] Alberto Girolami et al. “Modal analysis of structures with low-cost embedded systems”. In: *2018 IEEE International Symposium on Circuits and Systems (ISCAS)*. IEEE. 2018, pp. 1–4.
- [6] C Hall, R Andrews, and J Wuerker. *Fundamentals of Precision ADC Noise Analysis*. Tech. rep. Texas Instruments, Incorporated, 2020.
- [7] Hein Marais. “RS-485/RS-422 circuit implementation guide”. In: *AN-960 Analog Devices* (2008).
- [8] Gianfranco Piana et al. “Experimental modal analysis of straight and curved slender beams by piezoelectric transducers”. In: *Meccanica* 51.11 (2016), pp. 2797–2811.
- [9] Brian J Schwarz and Mark H Richardson. “Experimental modal analysis”. In: *CSI Reliability week* 35.1 (1999), pp. 1–12.
- [10] Stiny. *Aktive elektronische Bauelemente*. Springer Fachmedien Wiesbaden, 2019.
- [11] Tietze. *Electronic Circuits*. Springer Berlin Heidelberg, 2008.
- [12] Josef Vollmer et al. “Construction kit for low-cost vibration analysis systems based on low-cost acceleration sensors”. In: *2009 IEEE/ASME International Conference on Advanced Intelligent Mechatronics*. IEEE. 2009, pp. 463–468.
- [13] Chris Waltham and Andrzej Kotlicki. “Construction and calibration of an impact hammer”. In: *American Journal of Physics* 77.10 (2009), pp. 945–949.
- [14] Tong Wang et al. “Practical calibration techniques for the modal impact hammer”. In: *Sensors and Instrumentation, Volume 5*. Springer, 2015, pp. 23–29.

## Bibliography

- [15] John G Webster and Halit Eren. *Measurement, Instrumentation, and Sensors Handbook: Two-Volume Set*. CRC press, 2018.
- [16] Arthur Williams. *Analog filter and circuit design handbook*. McGraw Hill Professional, 2014.